





Kv3.1 and Kv3.3 subunits differentially contribute to Kv3 channels and action potential repolarization in principal neurons of the auditory brainstem

Nasreen Choudhury^{1,*}, Deborah Linley^{1,*}, Amy Richardson^{1,*}, Michelle Anderson¹, Susan W. Robinson³, Vincenzo Marra² , Victoria Ciampani¹, Sophie M. Walter¹, Conny Kopp-Scheinpflug⁴ , Joern R. Steinert¹  and Ian D. Forsythe¹ 

¹Auditory Neurophysiology Laboratory, Department of Neuroscience, Psychology & Behaviour, College of Life Sciences, University of Leicester, Leicester, LE1 7RH, UK

²Department of Neuroscience, Psychology & Behaviour, College of Life Sciences, University of Leicester, Leicester LE1 7RH, UK

³Neurotoxicity at the Synaptic Interface, MRC Toxicology Unit, University of Leicester, UK

⁴Division of Neurobiology, Department Biology II, Ludwig-Maximilians-University Munich, Großhaderner Strasse 2, Planegg-Martinsried, D-82152 Germany

Edited by: Kim Barrett & Walter Marcotti

Key points

- Kv3.1 and Kv3.3 subunits are highly expressed in the auditory brainstem, with little or no mRNA for Kv3.2 or Kv3.4. Changes in Kv3 currents and action potential (AP) firing were analysed from wild-type, Kv3.1 and Kv3.3 knockout (KO) mice.
- Both Kv3.1 and Kv3.3 immunostaining was present and western blots confirmed loss of subunit protein in the respective KO.
- Medial nucleus of the trapezoid body (MNTB) AP repolarization utilized Kv3.1 and/or Kv3.3; while in the lateral superior olive (LSO) Kv3.3 was essential.
- Voltage-gated calcium currents were unchanged between the genotypes. But APs evoked higher $[Ca^{2+}]_i$ in LSO than MNTB neurons; and were highest in the Kv3.3KO, consistent with longer AP durations.
- High frequency stimulation increased AP failure rates and AP latency in LSO neurons from the Kv3.3KO, underlining the physiological consequences for binaural integration.
- LSO neurons require Kv3.3 for functional Kv3 channels, while MNTB neurons can utilize either Kv3.1 or Kv3.3 subunits.

Nasreen Choudhury: has a PhD from the Indian Institute of Science, Bangalore; and came to Leicester to pursue her interest in potassium channels. She now works at Rush University Medical Centre, Chicago, to understand cortical dysfunction in Alzheimer's disease. **Deborah Linley:** has an MSc in Audiology from The University of Manchester, and a PhD from Leicester investigating activity-dependent changes in brainstem excitability. She is currently working at The University of Leeds, on the mechanosensitive ion channel Piezo1 and its role in human disease. **Amy Richardson:** Graduated from Leicester with a PhD studying the presynaptic roles of Kv3 channels. She continues her research into potassium channels and synaptic transmission in human disease models of epilepsy, based in the Neurology Dept, Queens Square, London.



*Contributed equally to this work

Abstract Kv3 voltage-gated potassium channels mediate action potential (AP) repolarization. The relative importance of Kv3.1 and Kv3.3 subunits for assembly of functional channels in neurons of the auditory brainstem was examined from the physiological perspective that speed and precision of AP firing are crucial for sound source localization. High levels of Kv3.1 and Kv3.3 mRNA and protein were measured, with no evidence of compensation by Kv3.2 or Kv3.4 in the respective knockout (KO) mouse. Using the KOs, composition of Kv3 channels was constrained to either Kv3.1 or Kv3.3 subunits in principal neurons of the medial nucleus of the trapezoid body (MNTB) and lateral superior olive (LSO); while TEA (1 mM) was employed to block Kv3-mediated outward potassium currents in voltage- and current clamp experiments. MNTB neuron APs (half-width 0.31 ± 0.08 ms, $n = 25$) were fast, reliable, and showed no distinction between channels assembled from Kv3.1 or Kv3.3 subunits (in the respective KO). LSO AP half-widths were also fast, but absolutely required Kv3.3 subunits for fast repolarization (half-widths: 0.25 ± 0.08 ms, $n = 19$ wild-type, 0.60 ± 0.17 ms, $n = 21$ Kv3.3KO, $p = 0.0001$). The longer AP duration increased LSO calcium influx and AP failure rates, and increased AP latency and jitter during high frequency repetitive firing. Both Kv3.1 and Kv3.3 subunits contribute to Kv3 channels in the MNTB (and compensate for each other in each KO); in contrast, LSO neurons require Kv3.3 subunits for fast repolarization and to sustain AP firing during high frequency stimulation. In conclusion, Kv3 channels exhibit both redundancy and Kv3.3 dominance between the brainstem nuclei involved in sound localization.

(Resubmitted 8 February 2020; accepted after revision 25 March 2020; first published online 4 April 2020)

Corresponding author I. D. Forsythe: Auditory Neurophysiology Laboratory, Department of Neuroscience, Psychology & Behaviour, College of Life Sciences, University of Leicester, Leicester LE1 7RH, UK. Email: idf@le.ac.uk

Introduction

Voltage-gated potassium channels are key regulators of neuronal excitability, action potential (AP) threshold, repolarization and waveform. Around 80 genes code for different K⁺ channel subunits, (Coetzee *et al.* 1999; Trimmer, 2015) where four alpha subunits assemble (usually from within the same family) to form each functional potassium channel. The four classic voltage-gated potassium channel families are: KCNA–D (Kv1–Kv4); each family has multiple alpha subunit genes, hence channels are often heterotetramers. Functional heterogeneity is further augmented by the inclusion of subunits from accessory protein families, beta subunits and secondary modifications, such as phosphorylation. The composition and complexity of ‘native’ channels vastly exceeds that of over-expressed ion channels in recombinant cell lines, hence understanding channel physiology requires investigation within specific systems, such as the auditory brainstem.

Here we focus on the classic ‘delayed rectifiers’ of the Kv3 family, which are comprised of four subunit-specific genes (*Kcnc1–4*). Kv3 channels are ‘high voltage-activated’ opening with the large depolarizations achieved only during an AP, and function to provide the repolarizing drive to minimise AP duration and maximise firing frequency. Kv3 genes are broadly expressed across the nervous system and are particularly associated with fast-spiking interneurons in the neocortex, hippocampus, striatum, cerebellum and the auditory brainstem (for

reviews, see Rudy *et al.* 1999; Kaczmarek & Zhang, 2017). Homomeric Kv3 channels have been well characterized by expression in recombinant systems (Grissmer *et al.* 1994; Macica & Kaczmarek, 2001; Desai *et al.* 2008), but in many brain regions multiple Kv3 subunit genes are expressed in the same neurons (Perney *et al.* 1992; Weiser *et al.* 1994; 1995; Chang *et al.* 2007), including neurons in the auditory brainstem. This has been taken as evidence of functional redundancy, since early studies of Kv3.1 knockouts (KOs) showed only a mild behavioural phenotype (with changes in cortical gamma and delta oscillations, Joho *et al.* 1999), while Kv3.3KOs showed no obvious behavioural phenotype (Espinosa *et al.* 2001). However, the double Kv3.1/3.3 KO showed a severe ataxia, tremor and myoclonus combined with hyperactivity, suggestive of multiple and differential regional dysfunction and consistent with broad utilization of these subunits in many neuronal types, which were particularly associated with fast-spiking interneurons (Chow *et al.* 1999; Lien & Jonas, 2003).

The central aim of this investigation was to test whether Kv3.1 and Kv3.3 subunits are each essential or functionally redundant for mediating fast AP repolarization, within different identified neurons in the auditory brainstem. This region lends itself to investigation since their principal neuron excitability and synaptic network have been well characterized. AP timing is crucial for binaural integration in sound source localization (Grothe, 2000; Tollin, 2003; Schnupp & Carr, 2009; Johnston *et al.* 2010; Franken *et al.* 2018; Kopp-Scheinplugg & Forsythe, 2018) and has physiological and behavioural consequences if disrupted.

In situ hybridization shows that both Kv3.1 and Kv3.3 are present in the auditory brainstem (Allen Mouse Brain Atlas; <http://mouse.brain-map.org>).

The auditory brainstem and the medial nucleus of the trapezoid body (MNTB) in particular, is a well-established model for studies of Kv3 channel physiology in the context of auditory processing. This investigation exploited KO mice to generate Kv3 channels of reduced complexity in this native physiological system, allowing the study of homomeric Kv3 currents in neurons which normally express multiple subunits. Whole-cell patch-clamp recordings in an *in vitro* brain slice preparation were used with transgenic mice, and combined with laser microdissection and quantitative RT-PCR to characterize high voltage-activated K⁺ currents in neurons of the MNTB and the lateral superior olive (LSO). The results show that Kv3.1 and Kv3.3 subunits are expressed, with little or no Kv3.2 and Kv3.4. In the LSO, Kv3.3 subunits were crucial for functional Kv3 channels and for generating short duration APs. In the MNTB, fast spiking was maintained in both Kv3.1 and Kv3.3 KO mice, implying that either subunit compensated for the absence of the other.

Materials and methods

Ethical oversight

Experiments were performed in accordance with the Animals (Scientific Procedures) Act (ASPA) 1986 and as revised by European Directive 2010/63/EU on the protection of animals used for scientific purposes. Experimental procedures were approved by the local ethical review committee and through a UK Home Office project licence.

Mouse strain sources. Experiments were conducted on wild-type and genetically modified mice, backcrossed onto a common inbred background strain of CBA/CaCrI (UK). This strain was selected as our wild-type (WT) strain because it has stable hearing and does not exhibit premature age-related hearing loss (Zheng *et al.* 1999).

The Kv3.1 KO mouse was originally generated on the 129/Sv background (Ho *et al.* 1997). These mice were backcrossed onto our CBA/CaCrI strain and maintained as a heterozygous breeding colony for more than 10 generations. The Kv3.3 KO mouse strain was originally generated on a C57BL/6 background (Espinosa *et al.* 2001) and was also backcrossed onto our CBA/CaCrI strain. These mice show no overt phenotype and were maintained initially as a homozygous breeding colony and currently as a heterozygous breeding colony. Genotyping was conducted using PCR of ear notch samples made at around P10.

All mice were housed, and breeding colonies maintained, in the Preclinical Research Facility at the University of Leicester, subject to a normal light/dark cycle of 12 h, with free access to food and water. Experiments employed male and female animals; qRT-PCR and histological studies were conducted on animals aged between P9 and P35; and electrophysiology from P14 to P25. The age range for each data set is as indicated in the figure and in the Statistical Summary Table.

Preparation of *in vitro* brain slices. For *in vitro* brain slice electrophysiology experiments, mice were killed by decapitation. The dissected brain was rapidly transferred to ice-cold artificial cerebrospinal fluid (aCSF) in which NaCl was substituted for equi-osmotic sucrose of composition (in mM): sucrose (250), KCl (2.5), NaHCO₃ (26), NaH₂PO₄ (1.25), D-glucose (10), ascorbic acid (0.5), MgCl₂ (4) and CaCl₂ (0.1). Transverse sections (150–200 µm thick) of the superior olivary complex (SOC) were prepared in the ice-cold aCSF using a vibroslicer (Campden Instruments, 7000smz).

Slices were allowed to recover in normal aCSF for 1 h at 37°C in a water bath and subsequently allowed to passively cool to room temperature. The normal aCSF was composed of (in mM): NaCl (125), NaHCO₃ (26), KCl (2.5), NaH₂PO₄ (1.25), myo-inositol (3), pyruvate (1), ascorbic acid (0.5), D-glucose (10), MgCl₂ (1) and CaCl₂ (2). All aCSF solutions were continually bubbled and saturated with 95% O₂ and 5% CO₂ gas mixture. External and internal osmolarities were respectively adjusted to be around 310 or 280 mOsM (approx., ±10 mOsM) using sucrose.

Whole-cell patch recording. For an experiment, one slice was placed in a recording chamber mounted on the stage of an upright microscope (Nikon Eclipse E600FN) and neurons visualized with a 60× DIC water immersion objective. The slice was continually perfused at a rate of 1 ml/min with normal aCSF and experiments were conducted at a temperature of 35(±1)°C. Whole-cell patch recordings were made using 1.5 mm OD × 0.86 mm ID glass capillaries (Harvard Apparatus) filled with an internal solution composed of (in mM): potassium gluconate (97.5), KCl (32.5), HEPES (5), EGTA (5), MgCl₂ (1) and K₂-ATP (2). pH was adjusted to 7.2 using KOH. Recordings were made using a Multiclamp 700B amplifier and pClamp 11 software (Molecular Devices, Sunnyvale, CA, USA) for electrophysiological data acquisition and analysis. Electrode and whole-cell capacitance were compensated, and series resistances (mean 9 MΩ, range 6–15 MΩ) were compensated by 70%. No leak subtraction was performed using the amplifier. Data were digitised at 20 kHz and filtered at 5 kHz. The stated voltages were not corrected for a liquid junction potential of –11 mV, using the above internal patch solution.

Voltage clamp: potassium currents. Neurons were voltage-clamped at a holding potential (HP) of -60 mV (unless stated otherwise) and current–voltage (I/V) relationships were generated over a range of -90 to $+40$ mV with 10 mV steps. Pharmacological tools are available, in that low millimolar concentrations of TEA block Kv3 channels in recombinant systems and native neurons (Grissmer *et al.* 1994; Brew & Forsythe, 1995; Wang *et al.* 1998; Macica & Kaczmarek, 2001; Desai *et al.* 2008). Our primary voltage command (see Fig. 1C) included a prepulse to -90 mV (for 200 ms) to remove steady-state inactivation and a second prepulse to -40 mV for 20 ms to inactivate voltage-gated

sodium channels and A-type potassium currents (if present). Calcium currents were measured on substitution in the aCSF of calcium chloride by barium chloride, and block of ionotropic receptors with DNQX ($10 \mu\text{M}$), D-AP5 ($20 \mu\text{M}$), bicuculline ($10 \mu\text{M}$) and strychnine ($0.5 \mu\text{M}$) to block synaptic activity from AMPA-, NMDA-, GABA_A⁻ and glycine receptors, respectively. Whole-cell patch recordings were made using pipettes filled with (in mM): CsCl (120); TEA-Cl (10); EGTA (1); HEPES (40); Na-phosphocreatine (5); Mg-ATP (2); Na-GTP (0.3). Neurons were held at a potential of -60 mV and allowed to equilibrate for 5 min before voltage step commands were applied in 10 mV increments. Only recordings where

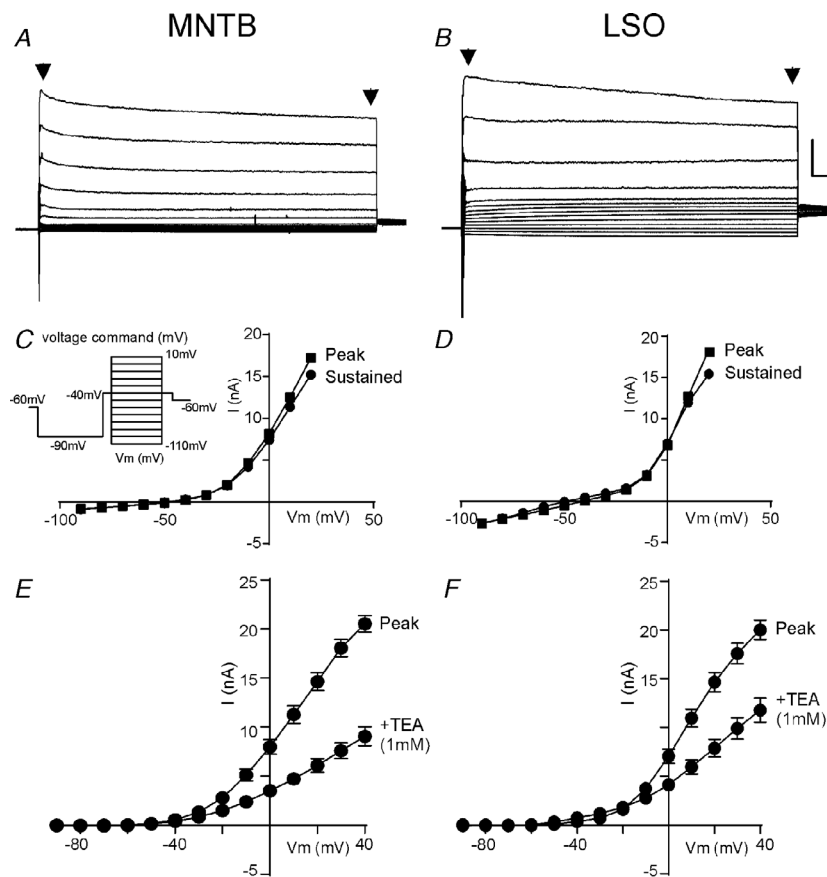


Figure 1. Whole-cell voltage clamp of currents from WT mice in MNTB (left) and LSO (right) principal neurons are of similar magnitude and time-course

Currents exhibit little inactivation, and block by TEA (1 mM) is consistent with a Kv3-mediated component. A and B, whole-cell voltage clamp from one MNTB (A) and one LSO (B) neuron show large outward currents in response to the voltage command illustrated below in part 1C. C and D, current–voltage (I/V) relationships for the single neurons (same ones as shown in 1A and 1B). Peak and sustained I/V s are plotted at the latency indicated by the arrows; the currents show a modest level of inactivation in both the MNTB and LSO. Note that LSO neurons possess a large current at voltage commands around rest; this is predominantly mediated by hyperpolarization-activated non-specific cation conductance (I_H). Inset in part C shows the voltage command protocol used for both MNTB and LSO neurons: HP = -60 mV, two pre-pulses, first to -90 mV (200 ms) to minimize inactivation and then -40 mV (20 ms) to inactivate voltage-gated sodium currents, prior to repeated I/V voltage commands to evoke outward potassium currents in 10 mV steps. E and F, leak-subtracted I/V s are plotted for 10 MNTB and 14 LSO neurons from WT mice; the mean \pm SEM is plotted to illustrate similar magnitude peak currents under control conditions (black) and for 5 MNTB neurons and 4 LSO neurons following extracellular perfusion of TEA (1 mM, red). Data from animals aged P14–P25.

the series resistance remained lower than 10 M Ω were analysed.

Action potential firing. Current clamp recordings were made from identified MNTB and LSO principal neurons. The membrane potential was adjusted to around -60 mV. APs were evoked using depolarizing step current injections lasting 200 ms; and the first evoked AP was analysed (Fig. 6) for neurons from each of the three genotypes. Measured parameters included AP amplitude, half-width and after-hyperpolarization. In order to examine the impact of Kv3 channel subunit composition on sustained AP firing in MNTB and LSO neurons (Fig. 10), APs were evoked by brief 0.3 ms depolarizing current injections over a range of frequencies (from 50–400 Hz). This input–output relationship was constructed for train durations of 500 ms and repeated at 30 s intervals for all frequencies. APs were triggered with depolarizing current steps (0.3 ms) of increasing magnitude from 0.5 to 3.5 nA. Trains were analysed to construct stimulus–response relationships, AP firing probability and AP timing with respect to the stimulus.

Calcium imaging. The imaging system consisted of Slidescope Pro 2000 microscope system (Scientifica UK),

fitted with FuraLED light source (Cairn Research Ltd, UK), powered by OptoLED (Cairn Research Ltd, UK) for fast optical switching and dual excitation of Fura-2 at 340 nm and 380 nm. A Prime BSI scientific CMOS camera (Photometrics) was used to capture the fluorescence signal obtained through a 510 nm emission filter. The wavelength switching by OptoLED and the camera were controlled digitally at 30 Hz per channel using pClamp 11 (Molecular Devices). Using μ Manager software (Open Imaging, Edelstein *et al.* 2014), multi-dimensional acquisition allowed hardware synchronization to obtain a dual-channel fluorescence signal at different time points at a rate of 30 Hz during the current injection protocol. Neurons (from the MNTB or LSO) were loaded with 50 μ M Fura-2 in the patch pipette containing (in mM): K⁺ gluconate (97.5), KCl (32.5), HEPES (40), EGTA (0.2), MgCl₂ (1), CaCl₂ (100), K₂-ATP (2.2), Na-GTP (0.3), pH 7.2 for 10 min after whole-cell configuration was established. Calcium signals are depicted as the ratio of fluorescence at 340 nm and 380 nm obtained during trains of 50 APs evoked at 100 Hz by postsynaptic current injection (1.5–3 nA for 0.3 ms). The peak ratio change in F_{340}/F_{380} (R_{peak}) relative to the baseline F_{340}/F_{380} (R_{baseline}), obtained from neurons in WT and KO animals, have been quantified as $(R_{\text{peak}} - R_{\text{baseline}})/R_{\text{baseline}}$, while the calcium transient decay was fit with a single exponential.

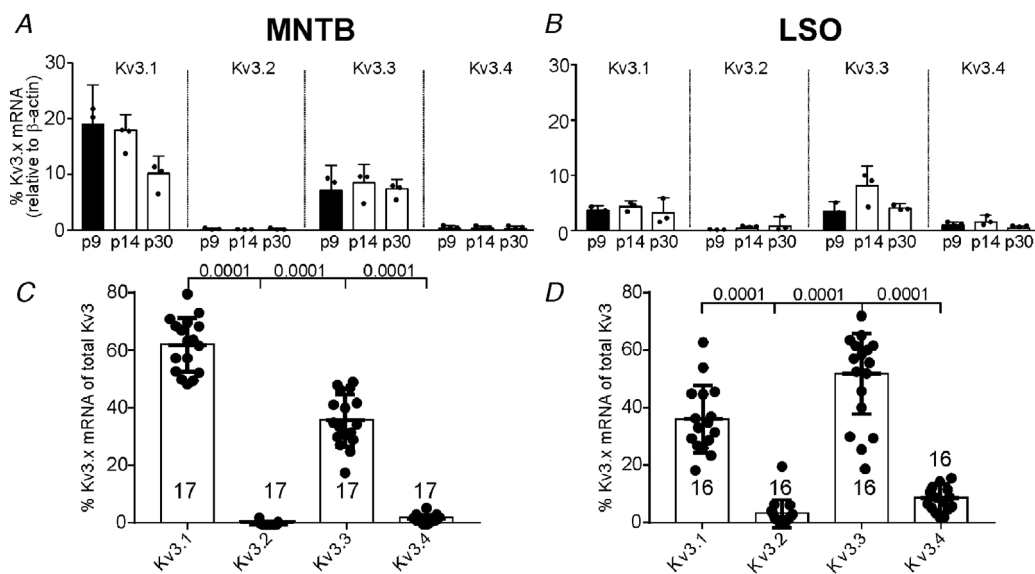


Figure 2. qRT-PCR of mRNA from MNTB and LSO shows dominance of Kv3.1 and Kv3.3, and low expression of Kv3.2 and Kv3.4

A and B, quantification of Kv3 gene mRNA is plotted relative to the housekeeping gene β -actin as bar graphs for three age groups: P9, P14 and P35 CBA/CaCrI mice. Tissue was micro-dissected from the MNTB and LSO, with individual data and mean \pm SD plotted for $n = 3$ mice in each age group. There is a clear predominance of Kv3.1 and Kv3.3 mRNA, but variance was high and no age-related changes were significant. C and D, the data for the above age groups were pooled and the experiment was repeated. The normalized data for each subunit relative to the total pool of Kv3 subunit mRNA are plotted for the MNTB and the LSO. The predominance of Kv3.1 and Kv3.3 mRNA over Kv3.2 and Kv3.4 is clear and statistically significant with P values indicated above paired comparisons for both nuclei. Statistical comparisons were conducted using two-way ANOVA with Tukey correction for multiple comparisons.

Western blots. Brainstem tissue was flash frozen on dry ice, stored at -80°C and on the day of use samples were submerged in 1% SDS and sonicated. Lysis buffer (Tris-HCl, pH 8.0 (20 mM); NaCl (150 mM); EDTA (5 mM) and 0.1% v/v Tween-20 with the protease inhibitors; leupeptin (10 $\mu\text{g/ml}$); aprotinin (1 $\mu\text{g/ml}$); anti-pain (10 $\mu\text{g/ml}$) and phenylmethylsulfonyl fluoride (PMSE, 1 mM) was added after sonication so that the final concentration of SDS was 0.1%. The protein concentration was measured using a Bio-rad protein assay. 50 μg protein was loaded into each well and subjected to SDS-PAGE. Subsequently, proteins were transferred to a nitrocellulose membrane, blocked for 1 h at room temperature in 5% milk, followed by a series of washing steps in TBS-tween (0.05%). They were then immunoblotted using a Kv3.1 antibody (NeuroMab, 75-041, AB2131480, monoclonal) at 1:500, and a Kv3.3 antibody at 1:1000 (Alomone, APC-102, Lot# AN0502, polyclonal) anti- β -actin at 1:1000 (Sigma A5441, Lot# 026M4780V, polyclonal). Protein bands were visualized in a FujiFilm LAS-4000 imager using primary antibodies, HRP-conjugated secondary antibodies and ECL reagents (GE healthcare). Fiji image analysis software was used for optical densitometric analysis of the protein bands, relative to β -actin.

Immunohistochemistry. Mice were killed by decapitation, their brains dissected and embedded in OCT (Thermo Scientific LAMB/OCT). The tissue was frozen rapidly in dry ice and Hexane and stored at -80°C . Tissue from at least three animals was used for each investigation; the

control background strain for all immunohistochemistry was CBA/CaCrI, onto which the Kv3.3KO and Kv3.1KO strains were backcrossed. Tissue was cryo-sectioned at 12 μm thick (Thermo, Cryostar NX50) onto poly D-lysine coated slides and stored at -20°C . Immediately before staining, slides were fixed using 4% paraformaldehyde (PFA) at 4°C for 10 min, washed 3×10 min in $1 \times$ PBS + 0.1% TritonX-100 (PBST). Antigen retrieval was performed in citric acid buffer (10 mM) pH6, at 95°C for 20 mins. Low affinity binding was blocked using 1% BSA + 10% normal goat serum (Vector Laboratories S-1000) in PBST ('blocking solution') for 1 h at room temperature. Primary antibodies, anti-Kv3.1b (1:1000; NeuroMab 75-041 Lot# 443.2KS.14b, monoclonal) and anti-Kv3.3 (1:3000; Alomone APC-102 Lot# AN0502, polyclonal), were diluted in blocking solution and incubated overnight at 4°C then washed 3×10 min in PBST. Secondary antibodies, 488 F(ab')₂ fragment of goat anti-mouse (1:1000 Invitrogen A11017) and 568 goat anti-rabbit IgG (H+L) (1:1000 Invitrogen A11036, polyclonal), were diluted in blocking solution and incubated at room temperature for 2 h. Slides were washed 3×20 min in PBST before cover slipping with hard-set mounting medium (Vectashield, H-1400) and stored at 4°C . Some sections were incubated without the primary antibody to test for non-specific immunostaining of the secondary Ab (data not shown) and pre-incubation with the antigenic peptide (blocking peptide) was conducted where the peptide was available. Immunostaining with Kv3.1b and Kv3.3 primary antibodies was confirmed as absent in the corresponding KO animals (see Fig. 3). Fluorescence

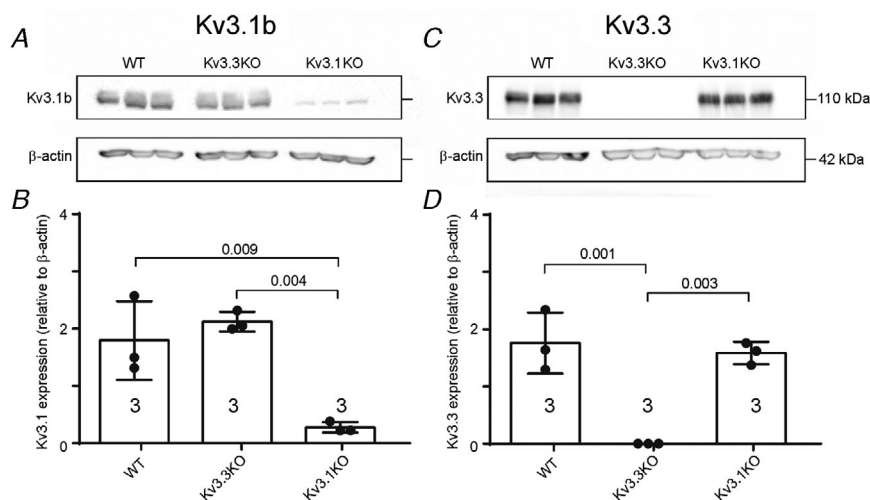


Figure 3. Western blots of protein extracted from brainstem tissue from each of the three genotypes: WT, Kv3.1KO and Kv3.3KO confirms lack of the appropriate subunit in the respective knockout

A, western blot for Kv3.1b and β -actin from brainstem tissue for 3 animals of each genotype. B, Optical density quantification of A showing lack of Kv3.1 in the Kv3.1KO mouse. C, western blot for Kv3.3Ab and β -actin from brainstem tissue for 3 animals of each genotype. D, quantification of C showing lack of Kv3.3 in the Kv3.3KO mouse. Individual and mean (\pm SD) protein measured as optical density relative to β -actin are plotted for $n = 3$ mice (aged P21); statistical comparisons were conducted using one-way ANOVA with Tukey correction for multiple comparisons, with P values as indicated on the bar graphs and in the Statistical Summary Table, Q5.

Table 1. Primer sequences

Kv3.1a	F- TCTGCAAAGCCTACGGATTC	R- AGGCTCAGCAAGGCTAAGG
Kv3.1b	F- CTTATCAACCGGGGAGTACG	R- AATGACAGGGCTTTCTTTGC
Kv3.2	F- GACCCGATGGCAAGTCAG	R- GAACAAAGAAGCAAAAGCAATAAA
Kv3.3	F- GACGTACCGCTCCACGTT	R- CCGGGTCGTAGTCAAAGC
Kv3.4	F- TCTTCGAGGATCCCTACTCATC	R- CGTTTCGGTCAATGTTGAAG
β-actin	F- GATTACTGCTCTGGCTCCTAGCA	R- GTGGACAGTGAGGCCAGGAT

imaging was conducted using a Zeiss Axio Observer microscope.

Quantitative RT-PCR. Tissue was obtained as detailed above for immunohistochemistry. Sections were obtained in the transverse plane at a thickness of 15–20 μ m onto membrane slides (Zeiss 1.0 PEN, cat# 415190-9041-000). Slides were fixed with 70% ethanol for 2 min at 4 $^{\circ}$ C, washed 3 \times for 1 min in nuclease-free water then stained for 1 min with Mayer Haematoxylin solution, washed in nuclease-free water and then dipped into 70% ethanol and 100% ethanol. Slides were then air-dried briefly. Microdissection of single nuclei of the SOC was carried out using laser microdissection (PALM laser system, Zeiss). Total RNA extraction was performed using an RNeasy tissue mini kit (Qiagen) and RNA was reverse-transcribed

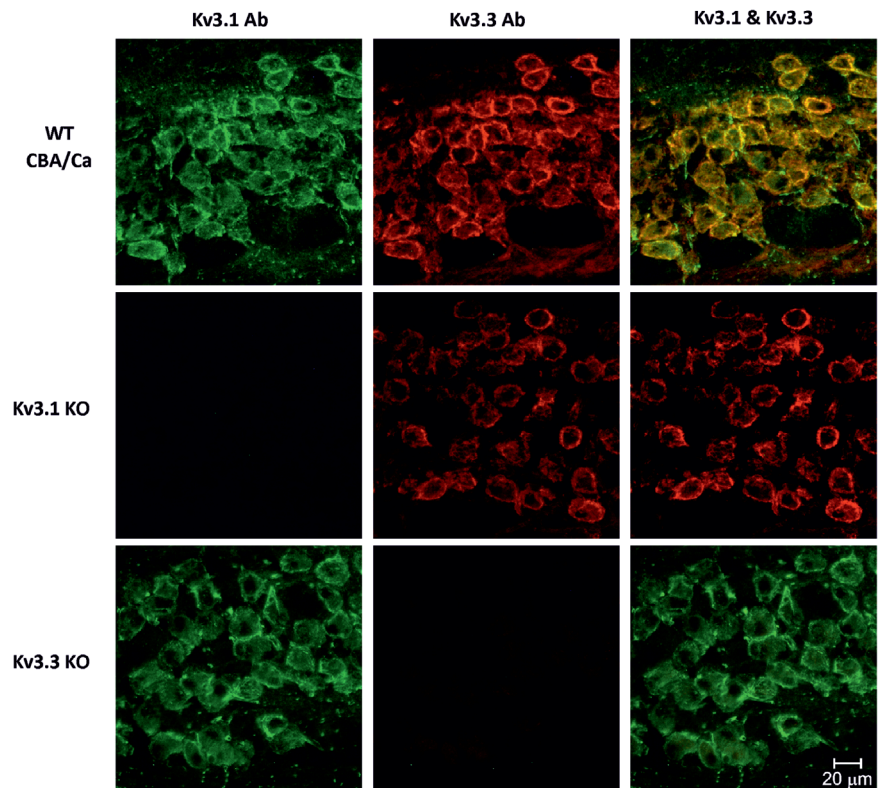
with SuperScript III (Invitrogen) using random hexamer primers (Promega). PCR primers were designed using the Universal Probe Library Assay Design Centre (Roche) and target specificity was confirmed using BLAST search (NCBI). Primers crossed exon-exon regions and the gene of interest was normalized against a housekeeping gene (β -actin) which is stably expressed across the sample groups.

qRT-PCR was performed using SYBR Green PCR Master Mix in the ABI PRISM 7700 Sequence Detection System, the thermal-cycler protocol was: stage one, 50 $^{\circ}$ C for 2 min; stage two, 95 $^{\circ}$ C for 10 min; stage three, 40 cycles at 95 $^{\circ}$ C for 15 s and 60 $^{\circ}$ C for 1 min. Each sample was run in triplicate. PCR results were analysed using the Pfaffl model for relative quantitation (Pfaffl, 2001).

Chemicals and drugs were purchased from Merck (UK) unless otherwise specified.

Figure 4. Co-immunostaining from WT mice shows labelling for both Kv3.1 and Kv3.3; and staining is absent from the respective knockout

The nine panel matrix shows co-immunolabelling of the MNTB by antibodies for Kv3.1b (left column, green) or Kv3.3 (middle column, red) and merged images for both Kv3.1 and Kv3.3 (right) in each of the three genotypes used for this study: the WT CBA/CaCrI mice (top row) exhibit co-immunolabelling with both Kv3.1 (green) and Kv3.3 (red) Abs. The Kv3.1KO (middle row) show no staining with the Kv3.1b antibody but red Kv3.3 Ab labelling is present in the same section. In the Kv3.3KO (bottom row) the Kv3.3 antibody fails to stain the MNTB, but green Kv3.1b Ab labelling is present in the same section. Mice were aged P20 and each immunohistochemical experiment was conducted on tissue from three mice of each genotype; representative images of MNTB neurons were taken at $\times 40$ magnification after co-staining with Anti-Kv3.1b and Anti-Kv3.3. Scale bar is 20 μ m.



Statistics and data presentation. Data summaries are presented as mean \pm SD (n) in the text. For electrophysiological recordings ' n ' is defined as the number of different neurons recorded from the specified animal genotype and environmental condition, and from at least three different animals. In the qRT-PCR and western blot data ' n ' was the number of animals; the immunofluorescence imaging was conducted from at least three animals in each genotype; calcium imaging data are presented as numbers of neurons imaged, from at least three animals in each genotype. In the figures, where possible and provided clarity could be preserved, raw data are plotted, in addition to the data summary. The programs used for numerical analysis and presentation were Excel (Microsoft Office) and Prism v7 (GraphPad Software). Detailed data summaries, the statistical test employed and the conclusion are presented in the Statistical Summary Table. The Gaussian distribution of data sets was confirmed using the Shapiro–Wilk normality

test. Two data subsets (one genotype out of the three, in Fig. 6B and 7D) were not parametric, and these statistics were re-tested with an ANOVA for non-parametric distributions (see Statistical Summary Table for detail).

Results

Three mouse genotypes were employed: CBA/CaCrI WT, CBA/CaCrI Kv3.1KO and CBA/CaCrI Kv3.3KO. Whole-cell patch-clamp recordings were made from MNTB or LSO principal neurons in an *in vitro* brain slice preparation prepared from CBA/CaCrI mice aged P14–P25. Voltage clamp experiments were conducted using the voltage command protocol shown as an inset in Fig. 1C, from a HP of -60 mV. Superimposed current traces from one MNTB and one LSO principal neuron are shown in Fig. 1A and B, with the current–voltage (I/V) relationship plotted for peak and sustained currents (arrows) in Fig. 1C and D, respectively. Principal neurons

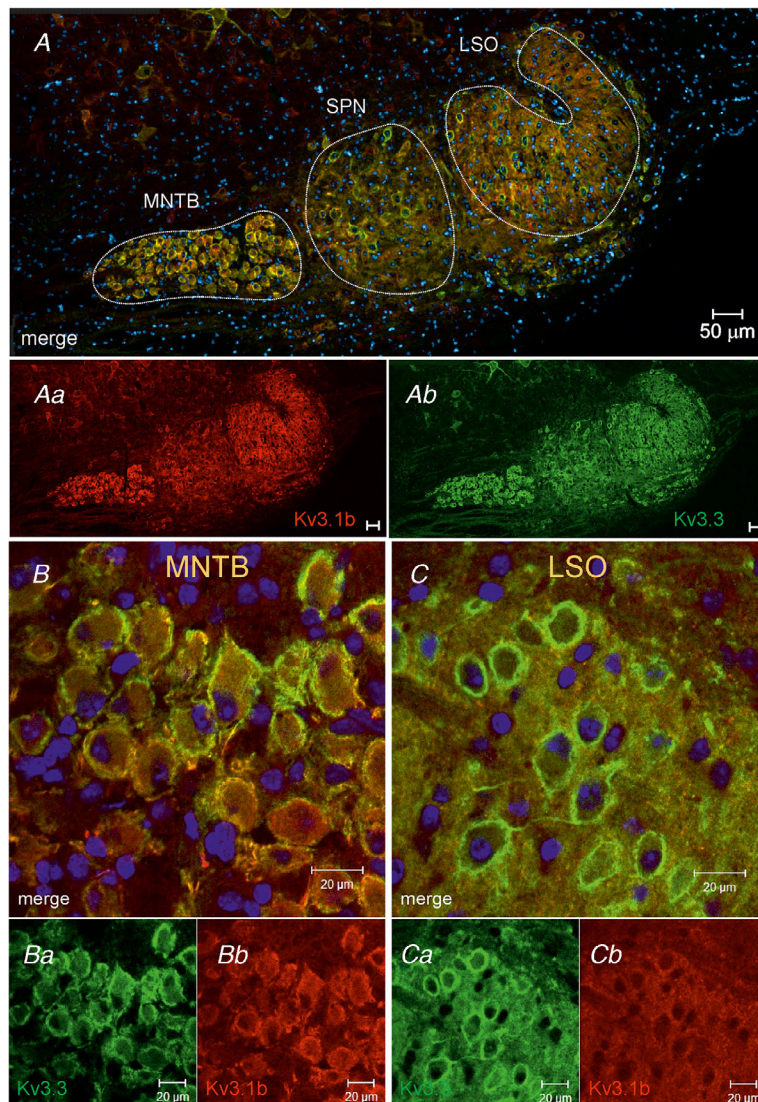


Figure 5. Kv3.1 and Kv3.3 immunostaining is distributed in neurons across the nuclei of the auditory brainstem, including the MNTB, the LSO and the superior paraolivary nucleus (SPN)
 A, co-immunolabelling for Kv3.1 (red) and Kv3.3 (green); cell nuclei are stained with DAPI (blue). The MNTB, SPN and the LSO are outlined with a dotted white line and labelled. All nuclei show extensive double labelling and are hence yellow in colour. The component images of immunostaining for Kv3.1b (red) and Kv3.3 (green) are shown below in Aa and Ab, respectively. Scale bar is 50 μ m. B, MNTB: high magnification images show extensive membrane and cytoplasmic staining for both Kv3.3 and Kv3.1b (the component images are shown below, in Ba and Bb). Scale bar is 20 μ m. C, LSO: high magnification images show extensive membrane and cytoplasmic staining for both Kv3.3 and Kv3.1b (the component images are shown below, in Ca and Cb). Scale bar is 20 μ m. Note the high level of neuropile staining in the LSO. Tissue was mice aged P20 and each experiment was conducted on three mice of each genotype, with representative images illustrated after co-staining with Anti-Kv3.1b and Anti-Kv3.3.

in the MNTB were recognised by their large soma (15–20 μm diameter) and single AP response to current injection (Brew & Forsythe, 1995; Wang *et al.* 1998; Johnston *et al.* 2008). Principal neurons of the LSO possess a prominent I_{H} – the hyperpolarization-activated non-specific cation conductance (Kopp-Scheinflug *et al.* 2015), and lack an A-current (Stereberg *et al.* 2010); see also Kopp-Scheinflug & Forsythe, 2018). The outward currents activated rapidly and exhibited partial inactivation during the 200 ms voltage command (Fig. 1A and B) as shown by comparing the current traces measured at the peak and the end (sustained) of the voltage command step (Fig. 1A and B).

Although the I/V relationships were similar for MNTB and LSO neurons, LSO neurons showed substantially greater 'resting' voltage-dependent current from -90 to -50 mV (compare Fig. 1A and B), consistent with an HCN1-mediated I_{H} current dominating the LSO resting conductance. MNTB neurons exhibit a slower HCN2-mediated I_{H} which activates at more negative voltages and contributes little to the resting conductance (Kopp-Scheinflug *et al.* 2015). Kv1 currents have been reported previously in the MNTB (Brew & Forsythe, 1995; Dodson *et al.* 2002) and LSO (Barnes-Davies *et al.* 2004). Application of Dendrotoxin-I (100 nM) to mouse MNTB and LSO neurons confirmed that Kv1 currents were of similar magnitude to those previously reported in rats with 0.9 ± 0.6 nA ($n = 4$) in MNTB neurons and 1.2 ± 0.3 nA ($n = 5$) in LSO neurons (voltage command step to -30 mV in the presence of 1 mM TEA. On average the response to a step voltage command to $+10$ mV generated large outward currents of magnitude 11.9 ± 1.2 nA (\pm SD, $n = 5$) and 14.6 ± 3.4 nA ($n = 11$) of similar magnitude in MNTB and LSO neurons (unpaired *t* test, $p = 0.118$; Statistical Summary Table, Q1).

MNTB and LSO neurons express Kv3.1 and Kv3.3 mRNA

Low concentrations of TEA substantially block whole-cell Kv3 current (Brew & Forsythe, 1995; Wang *et al.* 1998). The leak-subtracted I/V relationships are plotted for the peak outward current for control conditions (black trace) and during bath perfusion of 1 mM TEA (red trace) for MNTB and LSO neurons as shown in Fig. 1E and F, respectively. The Kv3-mediated TEA-sensitive outward K^+ current was measured as 4.0 ± 2.4 nA ($n = 5$) for MNTB neurons and 4.3 ± 0.5 nA ($n = 11$) at $+10$ mV and significantly differed from the respective WT control current amplitude (paired *t* test, $p = 0.04$ and 0.02 ; MNTB and LSO, respectively; Statistical Summary Table, Q2).

Previous studies have demonstrated that auditory brainstem neurons express Kv3.1 and Kv3.3 mRNA (Li *et al.* 2001), but their specific roles as Kv3 channel

subunits and respective functional importance are not clearly defined. Many publications have focused on Kv3.1 subunits; however, it is often difficult to clearly differentiate contributions from other Kv3 subunits to channel characteristics, especially in native neurons. Here we investigate which Kv3 subunits build Kv3 channels in the auditory brainstem and determine the extent to which the two subunits have differential roles.

We employed qRT-PCR to detect and quantify mRNA for the four Kv3 genes which might be expressed in the auditory brainstem. An additional issue was to ascertain if there were any significant changes in expression levels during maturation of the auditory pathway from P9 to P14 and P35. The data are expressed relative to a housekeeping gene (β -actin, Fig. 2A and B) for the MNTB and the LSO nuclei at each of three ages (P9, P14 and P35) and for the four genes (Kv3.1–Kv3.4) in the MNTB (Fig. 2A) and LSO (Fig. 2B). The variance of the Kv3 mRNA was high and no age-related or other differences were significant. For further analysis, data were integrated from the three age groups (each measured from different animals) giving $n = 9$; and the mRNA for each subunit was expressed as a percentage of the total for all four Kv3 subunits, in the respective nucleus. The raw data are shown for each animal and the bar shows the mean \pm SD. Kv3.1 mRNA was higher in the MNTB than in the LSO: 15.89 ± 5.74 versus 3.98 ± 1.45 ($n = 9$, $p = 0.0001$; Statistical Summary Table, Q3). In the MNTB, Kv3.1 and Kv3.3 mRNA levels were significantly higher than mRNA for Kv3.2 and Kv3.4 ($n = 9$, $p = 0.0001$) but the high variance and lower levels of mRNA in the LSO necessitated a repeat experiment, increasing n to 17 animals for the MNTB and to 16 for the LSO (Fig. 2C; also see Statistical Summary Table, Q4). Pooled data were normalized as a percentage of the total Kv3 mRNA in the respective nucleus. In the MNTB, Kv3.1 and Kv3.3 constituted 98% Kv3 mRNA, with low levels of mRNA for Kv3.2 or Kv3.4 (Kv3.1 > Kv3.3 >> Kv3.2 = Kv3.4). In the LSO, 88% of mRNA was for Kv3.1 and Kv3.3, where Kv3.3 > Kv3.1 >> Kv3.2 = Kv3.4. In both the MNTB and the LSO, Kv3.1 and Kv3.3 mRNAs were significantly higher than Kv3.2 and Kv3.4 ($p = 0.0001$).

The data show that Kv3.1 and Kv3.3 mRNAs dominate both the MNTB and the LSO. The results are also consistent with a mediolateral gradient of Kv3.1 mRNA across the SOC with the highest levels in the MNTB and lowest in the LSO. Further confirmation of the gradient was obtained by measuring Kv3 mRNA from the superior paraolivary nucleus (SPN) which lies between the MNTB and the LSO (see Fig. 5). Statistical analysis confirmed a mediolateral Kv3.1 mRNA gradient in that MNTB > SPN > LSO (Kv3.1: MNTB vs. SPN, MNTB vs. LSO, SPN vs. LSO: $p = 0.0001$, 0.0001 , 0.0123 ; respectively; Statistical Summary Table, Q4). There was also weaker evidence supporting a reciprocal gradient for Kv3.3, in that

the LSO had a higher proportion of Kv3.3 mRNA than the MNTB and SPN, although the SPN was not significantly different from the MNTB (Kv3.3; LSO vs. SPN, LSO vs. MNTB, SPN vs. MNTB: $p = 0.0449$, 0.0001 and 0.4953).

Inspection of the mean data for Kv3.2 and Kv3.4 mRNA in the LSO might suggest a higher proportion of these subunits than in the MNTB (the subunits constituting 2% and 12% of the total Kv3 mRNA, respectively). However, the variances were so great that the differences were not significant.

Transgenic mice lacking Kv3.1 or Kv3.3 showed no compensation by other subunits

Knockout mice for both Kv3.1 and Kv3.3 were obtained and backcrossed onto the CBA/CaCrI control strain (see Methods). The small size of the individual nuclei (see Fig. 5) precluded examination of protein levels in the single nuclei and so whole brainstem western blots were conducted to compare Kv3.1b and Kv3.3 protein levels in the control WT mice and KOs lacking either Kv3.1 or Kv3.3. Data are presented as optical density relative to the β -actin housekeeping gene. The antibodies detected bands at around 100 kD and 120 kD for Kv3.1b and Kv3.3 proteins, respectively (Fig. 3). Kv3.1b expression levels were measured as: ($n = 3$) WT: 1.8 ± 0.7 ; Kv3.1KO: 0.3 ± 0.1 , Kv3.3KO: 2.1 ± 0.2 ; Kv3.3 expression as ($n = 3$): WT: 1.8 ± 0.5 ; Kv3.1KO: 1.6 ± 0.2 , Kv3.3KO: 0.0 ± 0.0 . One-way ANOVA showed that in the Kv3.1KO, Kv3.1b protein was significantly reduced with respect to the WT ($p = 0.0093$) but the Kv3.3 protein level was unchanged ($p = 0.79$); and for the Kv3.3KO, Kv3.3 protein was significantly reduced with respect to the WT ($p = 0.0014$) but the Kv3.1b protein level was unchanged ($p = 0.615$). We conclude that deletion of Kv3.3 had no impact on Kv3.1 protein level, and no evidence for compensation was observed, in that the protein levels of Kv3.1 or Kv3.3 were unchanged in the respective KO. The potential for compensation by Kv3.2 or Kv3.4 mRNA levels were tested by measuring the levels of mRNA for the four Kv3 genes from the MNTB of both KO strains (Statistical Summary Table, Q6; P14, $n = 3$). The Kv3.1KO mouse had $3.10 \pm 0.98\%$ Kv3.1, $0.90 \pm 0.45\%$ Kv3.2, $93.9 \pm 29.7\%$ Kv3.3 and $2.09 \pm 0.14\%$ Kv3.4. The Kv3.3KO mouse had $87.10 \pm 20.36\%$ Kv3.1, $4.25 \pm 2.44\%$ Kv3.2, $0.04 \pm 0.04\%$ Kv3.3 and $8.61 \pm 2.45\%$ Kv3.4. In conclusion, for the Kv3.1KO, mRNA was predominantly Kv3.3 and for the Kv3.3KO mouse, mRNA was predominantly Kv3.1. There was no evidence for significant changes in Kv3.2 or Kv3.4 in either KO.

Further validation of the antibodies for Kv3.1b and Kv3.3 was conducted by examining the co-immunostaining in the MNTB from each genotype using the respective Kv3 antibodies as shown in Fig. 4.

The data are illustrated in a matrix format, with each row showing an example image from the respective genotype (WT, CBA/CaCrI; Kv3.1KO; Kv3.3KO) and each column showing the MNTB staining for the respective primary/secondary antibody (Kv3.1Ab, green; Kv3.3Ab, red; and the merged co-immunostaining). The result shows that immunostaining for both Kv3.1 and Kv3.3 was observed in WT MNTB, but specific staining was absent in the respective KO mouse strain. Representative images are shown from each genotype. The data also show that the two antibodies had little or no cross-reactivity.

Co-immunolabelling was employed to examine the distribution of Kv3.1 (red) and Kv3.3 (green) and nuclei (blue) labelling across the SOC, focusing on the MNTB and LSO. Fig. 5A shows the merged image of the SOC with broad distribution of staining across the nuclei; the two component images are shown below for Kv3.1b (Fig. 5Aa) and Kv3.3 (Fig. 5Ab). High magnification images show the principal neurons for the MNTB and LSO and are illustrated in Fig. 5B and 5C, respectively; with the single component images shown below the merged image (Figs 5Ba, 5Bb; 5Ca, 5Cb, respectively). Note that the MNTB staining is similar for both Kv3.1 and Kv3.3 with some cytoplasmic, but mostly high levels of membrane staining; the staining in the LSO is predominantly in the somatic membrane for Kv3.3 (green) while Kv3.1 (red) shows staining beyond the somatic membrane in the neuropil.

Resting neuronal parameters were broadly unchanged in the knockouts

Having established the distribution of Kv3 subunits and demonstrated that Kv3.1 and Kv3.3 are the predominant subunits that are localized across the SOC, we can now determine the contribution of these subunits to neuronal excitability.

Neuronal capacitance and input resistance for the MNTB and the LSO were unchanged between the genotypes, consistent with no gross changes in neuronal size or ion channel density (comparing WT vs. Kv3.1KO, and WT vs. Kv3.3 KO, respectively; see Summary Statistical Table, Qs 9 & 10). MNTB: WT = 11.8 ± 2.9 pF ($n = 9$), Kv3.1KO = 10.8 ± 1.9 pF ($n = 9$, $p = 0.9355$), Kv3.3KO = 10.5 ± 1.1 pF ($n = 10$, $p = 0.7949$); LSO: WT = 13.4 ± 2.2 pF ($n = 4$), Kv3.1KO = 11.3 ± 1.9 pF ($n = 7$, $p = 0.6012$), Kv3.3KO = 11.2 ± 2.2 pF ($n = 8$, $p = 0.5285$). Input resistances were measured from -60 mV for the MNTB: WT = 78.6 ± 19.0 MOhms ($n = 13$), Kv3.1KO = 66.8 ± 13.6 MOhms ($n = 6$, $p = 0.2798$), Kv3.1KO = 70.0 ± 11.4 MOhms ($n = 13$, $p = 0.3375$); LSO: WT = 17.7 ± 5.0 MOhms ($n = 17$), Kv3.1KO = 19.8 ± 4.0 MOhms ($n = 5$, $p = 0.5522$), Kv3.3KO = 17.2 ± 1.9 MOhms ($n = 14$, $p = 0.9359$). The input resistance of WT MNTB neurons at ~ 78 MOhms

was significantly greater than for WT LSO neurons at ~ 18 M Ω ($p = 0.0001$).

Current clamp measurements showed that the AP voltage threshold in the MNTB was -38.2 ± 6.7 mV ($n = 14$) in WT; -41.9 ± 3.2 mV ($n = 12$) in the Kv3.1KO and -36.3 ± 5.9 mV ($n = 11$) in the Kv3.3KO. In the LSO the voltage threshold was -34.6 ± 5.9 mV ($n=9$) in WT, and -41.6 ± 5.2 mV ($n = 11$) in the Kv3.1KO and -32.5 ± 6.8 mV ($n = 8$) in the Kv3.3KO. The threshold voltage in the LSO from the Kv3.1KO was significantly more negative than WT ($p = 0.035$; see Statistical Summary Table, Q11). The AP amplitudes showed no significant change between the genotypes (WT, Kv3.1KO and Kv3.3KO, measured from a membrane potential of -60 mV): MNTB: 61.1 ± 7.9 mV ($n = 14$), 59.5 ± 7.3 mV ($n = 11$), 57.8 ± 7.6 mV ($n = 11$); WT vs. Kv3.1KO and WT vs. Kv3.3KO were $p = 0.873$, $p = 0.544$, respectively. AP amplitude in the LSO were: 68.3 ± 6.3 mV ($n = 9$), 62.7 ± 9.5 mV ($n = 11$) and 73.9 ± 6.3 mV ($n = 7$); WT vs. Kv3.1KO and WT vs. Kv3.3KO were $p = 0.323$, $p = 0.901$, respectively, (see Statistical Summary Table, Q12). We conclude that there was no change in the AP amplitude in mice lacking Kv3.1 or Kv3.3. Since Kv3 channels are 'high voltage-activated' and particularly associated with AP repolarization, the next question was to compare AP durations from both the MNTB and LSO in WT, Kv3.1KO and Kv3.3KO mice, as shown in Fig. 6.

The Kv3.3 subunit was essential for fast APs in the LSO

The contribution of each Kv3 subunit to AP repolarization was assessed by measurement of AP half-width. For each genotype, example AP waveforms are shown in Fig. 6A for the MNTB (left) and LSO (right). The AP half-width duration data are plotted for all samples from each genotype in Fig. 6B, for MNTB (left) and LSO (right). In the WT, the half-width of both MNTB and LSO principal neurons is similar at 0.31 ± 0.08 ms ($n = 25$) and 0.25 ± 0.08 ms ($n = 19$). The respective KO means that Kv3 channels are dominated by the remaining subunit, so the Kv3.1KO will construct homomeric Kv3.3 channels, while the Kv3.3KO will have Kv3 channels predominantly composed of Kv3.1 subunits. In the MNTB, the AP duration increased similarly by around 0.1 ms for both KOs compared with WT (Kv3.1KO: 0.43 ± 0.09 ms, $n = 17$, $p = 0.0002$, vs. WT; Kv3.3KO: 0.44 ± 0.09 ms, $n = 18$, $p = 0.0001$, vs. WT). LSO AP half-width was unchanged in the Kv3.1KO, but were particularly slowed in the Kv3.3KO, suggesting that LSO neurons crucially depend on Kv3.3 subunits for fast repolarization (Kv3.1KO: 0.32 ± 0.08 ms, $n = 14$, $p = 0.2922$, vs. WT; Kv3.3KO: 0.60 ± 0.17 ms, $n = 21$, $p = 0.0001$, vs. WT). The increased duration was not due to changes in the rise time, with AP rise

time (10–90%): in the MNTB being 0.136 ± 0.017 ms ($n = 4$) in WT and Kv3.3KO, 0.172 ± 0.037 ms ($n = 7$, $p = 0.1076$, unpaired t test); and the LSO 0.157 ± 0.056 ms ($n = 7$) in WT and Kv3.3KO, 0.157 ± 0.051 ms ($n = 6$, $p = 0.9869$, unpaired t test; see Statistical Summary Table, Q15). Additional recordings from the SPN, which is located between the nuclei of MNTB and LSO, showed similar AP half-widths in WT which increased in both KOs (WT, Kv3.1KO & Kv3.3KO): 0.26 ± 0.3 ms ($n = 10$); 0.48 ± 0.17 ms ($n = 4$); 0.51 ± 0.10 ms ($n = 7$); and were significantly longer than WT in the respective KO ($p = 0.0031$; $p = 0.0001$), similar to the MNTB.

The change in depth of the after-hyperpolarizing potential (AHP) following each AP was unchanged in the MNTB: -10.9 ± 2.5 mV ($n = 14$), -9.0 ± 1.8 mV ($n = 11$), -9.6 ± 3.0 mV ($n = 11$); for WT, Kv3.1KO and Kv3.3KO, respectively (One-way ANOVA: WT vs. KO $p = 0.156$, $p = 0.404$). In the LSO the AHP amplitude was: -5.5 ± 2.8 mV ($n=10$), -4.8 ± 1.8 mV ($n = 11$), and

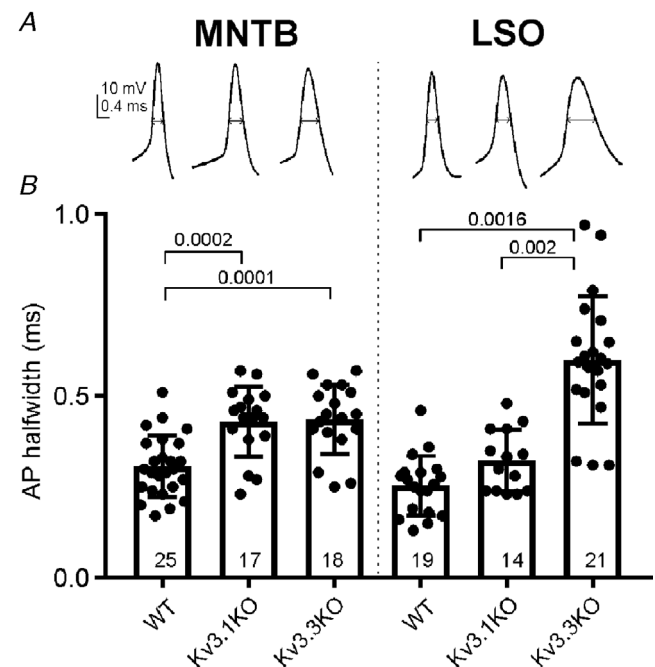


Figure 6. Action potential half-widths in the MNTB are increased in the Kv3.1KO and Kv3.3KO but in the LSO AP half-width is dramatically increased only in the Kv3.3KO

A, example current clamp recordings of evoked action potentials (APs) from MNTB (left) and LSO (right) principal neurons are shown for each of the three genotypes: WT, Kv3.1KO and Kv3.3KO. B, bar graphs showing the increase in AP half-width for the MNTB (left) and the LSO (right). APs have similar half-widths in the MNTB and LSO of WT mice. In the MNTB, half-widths increased on deletion of either Kv3.1 or Kv3.3 subunits. In the LSO, Kv3.3KO dramatically increased AP half-width, but Kv3.1 deletion has no effect. Individual data points and means \pm SD are plotted for each group, with n as indicated in each bar and P indicated above. Statistical significance was tested using a one-way ANOVA, with Tukey correction for multiple comparisons. Data from animals aged P14–P25.

-2.1 ± 1.4 mV ($n = 7$); for WT, Kv3.1KO and Kv3.3KO, respectively. One-way ANOVA: WT vs. KO $p = 0.990$, $p = 0.071$).

The deletion of Kv3.3 slowed LSO APs indicating that this subunit is essential in generating functional Kv3 channels in the LSO. However, both Kv3.1 and Kv3.3 subunits contributed to AP repolarization in the MNTB (and the SPN).

LSO outward currents required the Kv3.3 subunit

The next question was to investigate the extent to which outward potassium currents of MNTB and LSO principal neurons are influenced by deletion of the Kv3.1 or Kv3.3

gene. Superimposed raw current traces (no leak subtraction, using the voltage clamp protocol illustrated in Fig. 1C) from each genotype (WT, Kv3.1KO and Kv3.3KO) for one representative MNTB and LSO principal neuron are shown in Fig. 7A and E, respectively. In general, the WT outward currents were similar in the MNTB and the LSO (with the only major difference being I_H , as noted previously). Currents from the Kv3.1KO were indistinguishable from WT MNTB and LSO neurons, exhibiting similar magnitude peak currents and modest levels of inactivation. In the Kv3.3KO, currents in the MNTB were indistinguishable from WT, but LSO currents were of smaller magnitude and exhibited little or no inactivation (Fig. 7).

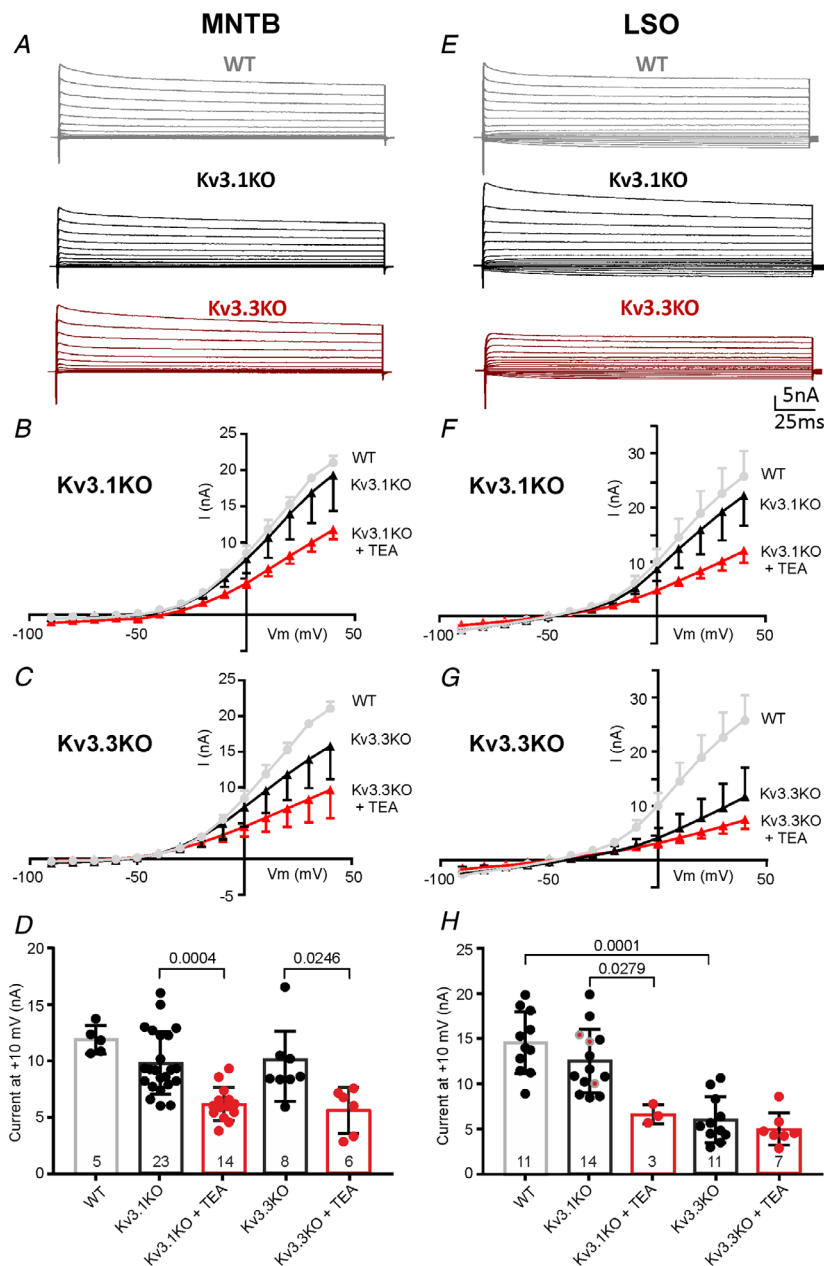


Figure 7. Kv3.3 subunits are crucial for LSO outward currents. Comparison of the I/V relationships for MNTB and LSO neurons from each genotype: WT, Kv3.1KO and Kv3.3KO

A, MNTB example traces from voltage commands from -90 to $+40$ mV are shown for each genotype, as labelled. E, LSO, example traces from voltage commands from -90 to $+40$ mV are shown for each genotype as labelled. B and C, mean (\pm SD) I/V curves of peak currents for MNTB principal neurons, from the Kv3.1KO and the Kv3.3KO, respectively. F and G, mean (\pm SD) I/V curves for peak currents for LSO principal neurons, from the Kv3.1KO and the Kv3.3KO, respectively. WT data are overlaid with I/Vs from each knockout and following block of Kv3 channels by 1 mM TEA for both cell types, as indicated in parts B, C, F, G. Note that the WT data (grey symbols and line) is the same in B and C, and in F and G (to aid comparison). D and H, bar graphs of the mean (\pm SD) outward peak currents evoked on voltage command to $+10$ mV for the indicated genotype and neuron type. In the Kv3.1KO the outward currents are not significantly different from WT MNTB or LSO neurons and TEA (1 mM) still blocks a significant outward current component. The control data for the three MNTB neurons in the Kv3.1KO that received TEA are indicated in grey. The result is similar for the MNTB in the Kv3.3KO; however, in LSO neurons from the Kv3.3KO, the KO has much lower outward current and the TEA (1 mM) block is small and not significantly different from the Kv3.3KO without TEA. The number of neurons for each condition and the results of a two-way ANOVA (with Tukey correction) is presented for the MNTB and LSO, respectively (see Statistical Summary Table). Each I/V is plotted without leak subtraction for MNTB (B and C) and LSO principal neurons (F and G). Data from animals aged P14–P25.

Whole-cell voltage clamp was used to test the extent to which outward currents in each genotype were blocked by 1 mM TEA. The mean I/V relationships (unpaired data, without leak subtraction) are plotted in Fig. 7B and C and Fig. 7F and G for the MNTB and LSO, respectively. The overlaid WT I/V (grey symbols) for the MNTB and LSO is copied in both I/V curves (Fig. 7B and C MNTB, and Fig. 7F and G LSO, respectively) to permit comparison with the KO I/Vs and for comparison with the data following addition of 1 mM TEA to block Kv3 currents.

Data were summarized and ANOVA statistical analyses were applied to the peak amplitude of the outward currents at a voltage command of +10 mV and these are plotted in the bar graphs in Fig. 7D and Fig. 7H for the MNTB and LSO, respectively. In the MNTB, KO of either Kv3.1 or Kv3.3 had no significant impact on current amplitude, while TEA significantly blocked the remaining current in both KOs to a similar extent (Figs 7B, C and D). MNTB peak currents at +10 mV for WT were 11.9 ± 1.2 nA ($n = 5$); Kv3.1KO: 9.8 ± 2.8 nA ($n = 23$); Kv3.3KO: 10.1 ± 3.0 nA ($n = 7$) and on perfusion of TEA the outward currents were 6.1 ± 1.4 nA ($n = 14$) for the Kv3.1KO ($p = 0.0003$); and 5.6 ± 2.0 nA ($n = 6$) for the Kv3.3KO ($p = 0.009$; Statistical Summary Table Q19). These results show that MNTB neurons generated Kv3 channels from the remaining subunit, in the absence of either Kv3.1 or Kv3.3.

In the LSO, KO of Kv3.1 had no effect on the I/V, but data from the Kv3.3KO showed dramatically reduced outward currents ($p = 0.0001$, Fig. 7G and H). In contrast to the MNTB, TEA had no further effect on the LSO currents from the Kv3.3KO, but TEA significantly reduced the LSO outward currents in the Kv3.1KO ($p = 0.0279$, Fig. 7F and H). LSO peak currents at +10 mV for WT: 14.6 ± 3.4 nA ($n = 11$); Kv3.1KO: 12.5 ± 3.5 nA ($n = 14$); Kv3.3KO: 6.0 ± 2.5 nA ($n = 11$) and on perfusion of TEA the outward currents were Kv3.1KO: 6.6 ± 3.0 nA ($n = 3$); Kv3.3KO: 5.0 ± 1.8 nA ($n = 11$).

Focusing on the averaged data for the MNTB (Fig. 7D bar graphs) statistical analysis (ANOVA) showed that TEA blocked a similar sized Kv3 current from both the Kv3.1KO and the Kv3.3KO. In the LSO (Fig. 7H bar graphs) the outward currents in the WT and Kv3.1KO were not significantly different, consistent with an interpretation that Kv3.1 had little or no role in the LSO; while the block by TEA in the Kv3.1KO, shows that the LSO Kv3 current was likely mediated by Kv3.3 subunits. This interpretation was confirmed by the small magnitude of the LSO outward current in the Kv3.3KO, and the absence of any further block by TEA. This further indicates that no other TEA-sensitive subunit (such as Kv3.2 or Kv3.4) had compensated for the absence of Kv3.3, consistent with the qRT-PCR data (above).

The MNTB Kv3 currents are mediated by channels composed of either Kv3.1 or Kv3.3 subunits. In the LSO,

Kv3 currents cannot be sustained by Kv3.1 alone, and Kv3.3 subunits must be present to form functional channels. The absence of a significant TEA-sensitive component in the LSO from the Kv3.3KO is consistent with little or no compensation by other Kv3 subunits.

Steady-state inactivation of the Kv3 currents

Under physiological conditions during high-frequency synaptic stimulation, which can exceed 100 Hz, MNTB and LSO membrane potentials depolarize from around -60 mV to -40 mV (for example, see synaptic trains in Lucas *et al.*, 2018). Such depolarization may induce steady-state inactivation of the Kv3 current. To test whether Kv3 channels exhibit steady-state inactivation, we compared the I/Vs generated from holding potentials of -60 and -40 mV using the voltage commands illustrated in Fig. 8A (inset). In WT MNTB the I/Vs are superimposed and there is no significant difference in the currents evoked from HP of -60 mV or -40 mV (Fig. 8A). In WT LSO neurons the same voltage command showed a modest reduction in outward current indicating some steady-state inactivation (Fig. 8E). The experiment was repeated in both Kv3.1KO and Kv3.3KOs and steady-state inactivation tested by comparing the outward current amplitude at a voltage command of +10 mV in each genotype, which is plotted in Fig. 8D and Fig. 8H for the MNTB and LSO, respectively. MNTB neuron peak currents at +10 mV were: WT -60 mV: 9.59 ± 2.37 nA ($n = 6$); WT -40 mV: 8.53 ± 1.87 nA ($n = 6$); Kv3.1KO -60 mV: 6.19 ± 1.74 nA ($n = 6$); Kv3.1KO -40 mV: 4.45 ± 1.11 nA ($n = 6$); Kv3.3KO -60 mV: 7.58 ± 2.19 nA ($n = 6$); Kv3.3KO -40 mV: 5.58 ± 1.24 nA ($n = 6$). In the LSO, neuron peak currents at +10 mV were: WT -60 mV: 11.68 ± 2.59 nA ($n = 6$), WT -40 mV: 7.46 ± 2.04 nA ($n = 6$); Kv3.1KO -60 mV: 8.76 ± 1.62 nA ($n = 6$), Kv3.1KO -40 mV: 6.63 ± 1.18 nA ($n = 6$); Kv3.3KO -60 mV: 5.25 ± 0.98 nA ($n = 6$), Kv3.3KO -40 mV: 3.61 ± 0.66 nA ($n = 6$). Two-way ANOVA analysis showed a statistical difference between the currents evoked from -60 and -40 mV only in WT LSO neurons ($p = 0.0011$, see Statistical Summary Table, Q16), thus there is little evidence that incorporation or omission of Kv3.1 or Kv3.3 subunits from Kv3 channels has a significant impact on steady-state inactivation.

Longer APs evoked greater voltage-gated calcium influx in the LSO

One consequence of longer duration APs would be to increase calcium influx through voltage-gated calcium channels and raised $[Ca^{2+}]_i$. Activity-dependent increases in intracellular calcium in MNTB and LSO neurons were observed using postsynaptic trains of 50 APs, delivered at 100 Hz. Postsynaptic APs were evoked by injection of brief currents (0.3 ms) to trigger APs in MNTB and

LSO principal neurons from the WT, Kv3.1KO and the Kv3.3KO mouse strains. Changes in soma $[Ca^{2+}]_i$ were measured using Fura-2 loaded by diffusion from the patch pipette. The rise in $[Ca^{2+}]_i$ was compared using the peak $\Delta F/F$ ratio in response to AP stimulation across the three genotypes, with traces overlaid in Fig. 9A (MNTB, left; LSO, right). The peak changes are plotted in the bar graphs below in Fig. 9B. MNTB WT: 0.169 ± 0.102 ($n = 6$), Kv3.1KO: 0.142 ± 0.047 ($n = 6$), Kv3.3KO: 0.272 ± 0.078 ($n = 6$). LSO WT: 0.353 ± 0.129 ($n = 6$), Kv3.1KO: 0.396 ± 0.19 ($n = 6$), Kv3.3KO: 1.038 ± 0.177 ($n = 6$). There was no statistically significant difference in the $\Delta F/F$ ratio for MNTB neurons between the genotypes, consistent with the small increase in AP duration in these neurons. However, in the LSO the peak $\Delta F/F$ ratio for

Kv3.3KO was significantly larger than the WT ($p = 0.0001$) and the Kv3.1KO ($p = 0.0001$), consistent with the large increase in AP duration in the LSO neurons of the Kv3.3KO. Examination of the exponential decay tau (rate of recovery) is plotted in Fig. 9C for intracellular calcium following the 50AP; this was also unchanged in the MNTB between the genotypes, but was significantly slower in the LSO of the Kv3.3KO ($p = 0.032$; Statistical Summary Table, Q20).

It was conceivable that the raised $[Ca^{2+}]_i$ observed in the above experiments could be due to a compensatory increase in the magnitude of postsynaptic voltage-gated calcium currents in LSO neurons from the Kv3.3KO. So, we directly measured the magnitude of the voltage-gated divalent current in MNTB and LSO neurons using barium

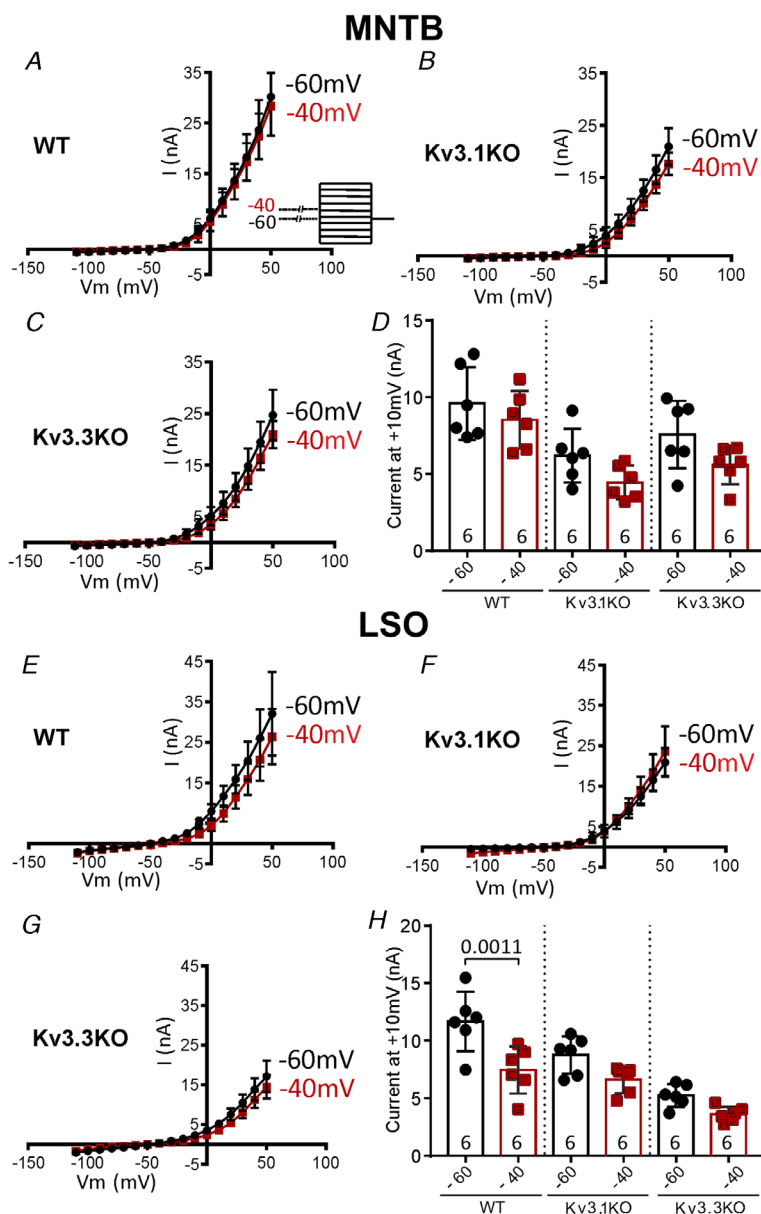


Figure 8. Comparison of steady-state inactivation in the MNTB and LSO in WT and in the Kv3.1KO or Kv3.3KO

The current I/V relations were compared from holding potentials of -60 mV (black) or -40 mV (red) for both MNTB (A–D) and LSO (E–H) neurons in each of the three genotypes. A, I/V for WT MNTB on holding at either -60 or -40 mV. B, I/V for Kv3.1KO MNTB on holding at either -60 or -40 mV. C, I/V for Kv3.3KO MNTB was similar on holding at either -60 or -40 mV. D, summary bar graph plotting MNTB-evoked currents on stepping to $+10$ mV from the respective steady-state holding potential of -60 or -40 mV for WT, Kv3.1KO or Kv3.3KO. There were no statistically significant changes within the different genotypes on shifting the holding potential from -60 to -40 mV. E, I/V for WT LSO on holding at either -60 or -40 mV. F, I/V for Kv3.1KO LSO on holding at either -60 or -40 mV. G, I/V for Kv3.3KO LSO was similar on holding at either -60 or -40 mV. H, summary bar graph plotting LSO-evoked currents on stepping to $+10$ mV from the respective steady-state holding potential of -60 or -40 mV for WT, Kv3.1KO or Kv3.3KO. There was a significant reduction in steady-state inactivation between -60 and -40 mV in WT LSO neurons ($p = 0.0011$), but not between the knockout genotypes. Data from animals aged P14–P25.

as the charge carrier. The I/Vs are plotted for each of the genotypes in Fig. 9D; the currents evoked from MNTB (left) and the LSO (right) neurons are overlaid. The peak magnitude of the inward barium currents were measured at -10 mV and plotted in the bar graph in Fig. 9E. The mean data are: MNTB, WT: 1.2 ± 0.2 nA ($n = 6$); Kv3.1KO: 1.0 ± 0.2 nA ($n = 7$); Kv3.3KO: 1.2 ± 0.2 nA ($n = 6$); LSO, WT: 1.6 ± 0.4 nA ($n = 10$); Kv3.1KO: 1.6 ± 0.2 nA ($n = 6$); Kv3.3KO: 2.0 ± 0.1 nA ($n = 7$). Within the MNTB and LSO, two-way ANOVA analysis of divalent current magnitudes showed no statistical differences between the genotypes in the MNTB or LSO; but the divalent current magnitudes were larger in the

LSO than the MNTB: WT, MNTB vs. LSO, $p = 0.0147$; Kv3.1KO, MNTB vs. LSO $p = 0.0031$; Kv3.3KO, MNTB vs. LSO $p = 0.0001$ (Statistical Summary Table, Q21). The data support the idea that the increase in intracellular calcium on Kv3.3 deletion in LSO principal neurons is a direct consequence of longer APs, rather than an indirect effect on voltage-gated calcium channels.

A potential contribution from calcium-dependent potassium channels was determined by comparing the I/V relationship in aCSF with normal (2.0:1.0 mM) and low (0.1:2.9 mM) $[Ca^{2+}]_i$: $[Mg^{2+}]_i$ calcium concentrations. The current at $+10$ mV was not significantly different in MNTB neurons: 11.1 ± 2.2 nA ($n = 5$); 10.0 ± 2.4 nA

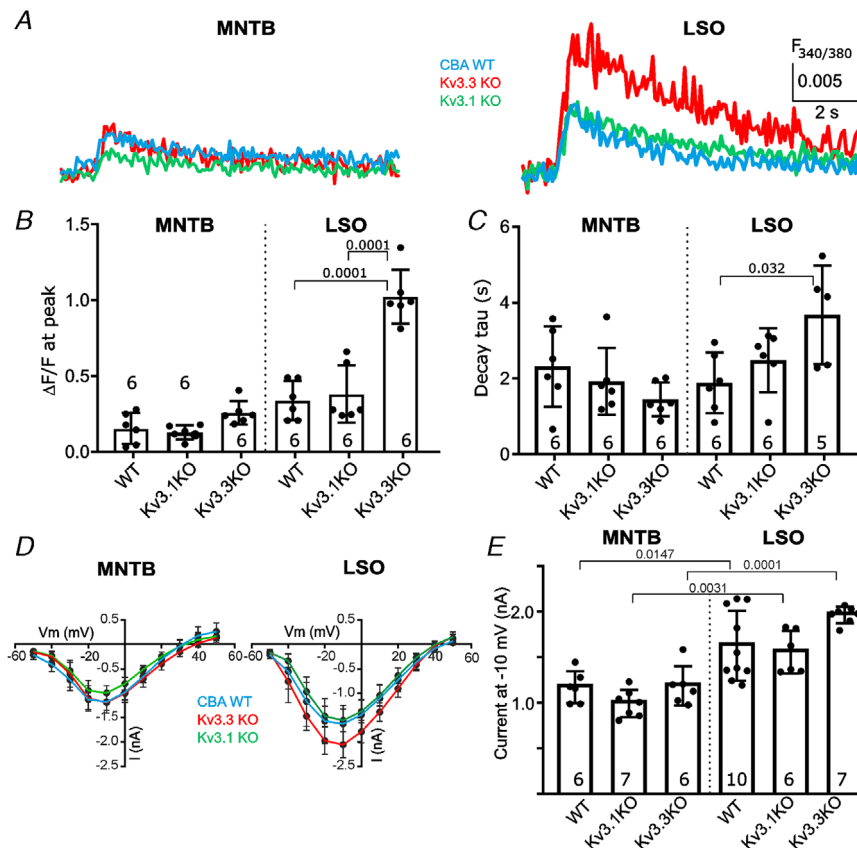


Figure 9. Somatic imaging of $[Ca^{2+}]_i$ shows that the longer AP duration increases peak intracellular calcium load of LSO neurons in the absence of Kv3.3

A, plot of Fura2 fluorescence ratio (340/380 nm) against time for neurons in the MNTB (left) and LSO (right) following 50 APs @100 Hz stimulation for the three genotypes: CBA/CaCr1 WT (black), Kv3.1KO (green) and Kv3.3KO (red). B, bar graphs show change in $\Delta F/F$ ratio at the peak, for MNTB and LSO neurons; there is a significant increase in the fluorescence ratio observed for Kv3.3KO in the LSO compared with WT, but not for the Kv3.1KO. The changes in the MNTB were not significantly increased in either KO. C, the decay kinetics of the $\Delta F/F$ ratio were fit by a single exponential of around 7 s; this was similar between the MNTB and LSO neurons, and it slowed significantly ($p = 0.032$) only in LSO neurons from the Kv3.3KO genotype. D, the magnitude of voltage-gated calcium channel current was estimated using barium as the charge carrier. Superimposed I/Vs for MNTB and LSO neurons from each genotype are shown: WT (black), Kv3.1KO (green) and Kv3.3KO (red). N is as stated in the bar graphs in part E. E, bar graph of peak inward barium current at -10 mV command for each genotype. WT LSO neurons had larger voltage-gated barium currents than MNTB neurons, but there were no significant differences between the genotypes (WT, Kv3.1KO, Kv3.3KO) in either the MNTB or the LSO. Data from animals aged P18–P25.

($n = 5$) $p = 0.5018$; while currents from LSO neurons were 11.0 ± 1.1 nA ($n = 5$); 6.8 ± 2.2 nA ($n = 5$) $p = 0.0116$; suggesting that calcium-dependent potassium currents could contribute to repolarization in the LSO in the absence of Kv3 channels (Statistical Summary Table, Q18).

LSO AP firing rates declined, while latency increased in the Kv3.3KO

The physiological relevance of Kv3.1 and Kv3.3 subunits was tested by comparing the ability of principal neurons to sustain AP firing across a range of firing frequencies in the WT, Kv3.1KO and Kv3.3KO genotypes. The I/V data

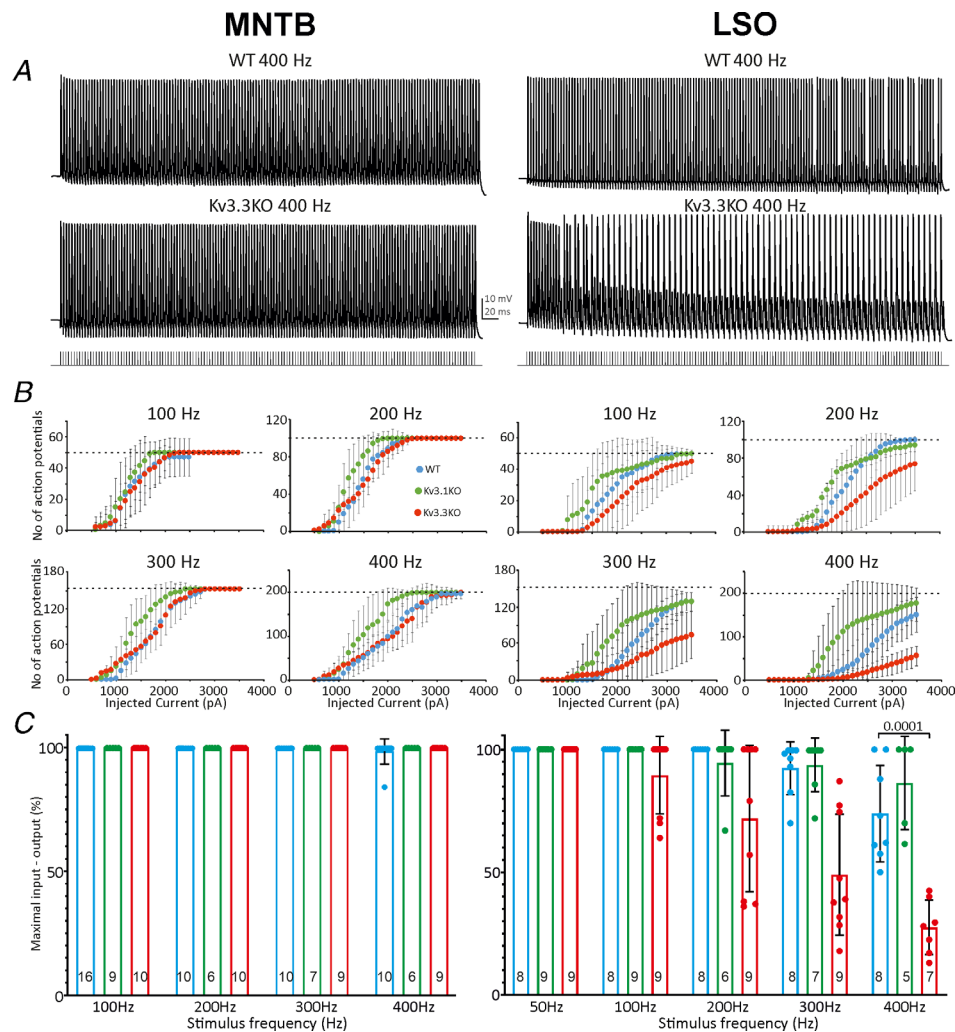


Figure 10. Stimulus–response curves for MNTB and LSO show that high frequency firing is compromised in LSO neurons from Kv3.3KO mice

A, example traces showing the AP firing response to 400 Hz stimulation from MNTB (left) and LSO neurons (right) in WT (upper trace) and Kv3.3KO (middle trace) genotypes; current injection stimulus is displayed as vertical lines in the lower trace. B, the stimulus–response curves are presented as the mean (SD) number of evoked APs plotted against the magnitude of the injected current stimulus, for the MNTB (left) and LSO (right) at four frequencies: 100, 200, 300 and 400 Hz. The data for each genotype are superimposed on the graph for the respective frequency: WT (blue), Kv3.1KO (green) and Kv3.3KO (red). The dotted line indicates the maximum number of evoked APs for the stated frequency of stimulation. The n for each curve is the same as that indicated in the bar graphs in part C. A summary of the stimulus–response data is plotted, with the bar graphs showing the percentage maximal input–output (i.e. successful AP firing) for each genotype (WT, blue; Kv3.1KO, green; Kv3.3KO, red) for the MNTB (left, 100–400 Hz) and LSO (right, 50–400 Hz). The MNTB shows only one ‘failure’ (WT @400 Hz); while the WT LSO failures increased above 200 Hz, with the Kv3.3KO showing the highest levels of firing failure. Note that data sets with identical values precluded statistical tests; distribution normality was tested using the Shapiro–Wilk test; then two-way ANOVA; N is indicated in each bar and also applies to B. See the Statistical Summary Table for details. Data from animals aged P14–P25.

shows that Kv3.3 subunits are dominant in LSO principal neurons and therefore AP firing should be more prone to failure as firing frequency increases. Stimulus–response relationships were generated over a frequency range of 50 to 400 Hz (using trains lasting 500 ms) to test this hypothesis.

Recordings were made from single neurons, stimulated at 50, 100, 200, 300 or 400 Hz using 0.3 ms current steps. Evoked AP trains at 400 Hz are plotted for the MNTB (left) and the LSO (right) in Fig. 10A; these raw traces are shown for WT and Kv3.3KO mice, only. The full data set was plotted as stimulus–response curves for each frequency and across the three genotypes, for the MNTB (left) and the LSO (right) in Fig. 10B (WT, blue; Kv3.1KO, green; and Kv3.3KO, red). The dashed line in each plot indicates the maximum output (when each stimulus generated an AP) and the peak AP firing achieved for that stimulus frequency. These data are summarized as percentage maximum input–output in the bar graphs in Fig. 10C (where the numbers in each bar indicate *n* for the data in Figs 10B and C). In the MNTB, the maximum response firing was achieved for every stimulus across a 100–400 Hz range in each genotype, with only one WT MNTB neuron failing at 400 Hz (Fig. 10C, blue bars). In the LSO, maximum response firing in all genotypes was achieved only at 50 Hz (Fig. 10C, right). WT LSO neurons sustained maximal firing to 200 Hz, while in the Kv3.1KO they sustained firing to 100 Hz. In the Kv3.3KO maximal firing rates declined with increasing frequency, and averaged less than 30% at 400 Hz (raw data in Fig. 10A, lower right trace; 10B lower right red graph; 10C, far right red bar; for full data set and p values see Summary Statistical Table, Q23). Normally distributed data for the percent maximal input–output firing of LSO neurons in Kv3.3KO at 400Hz was compared to 400Hz in WT (by an unpaired t-test). Stimulation at 400Hz in the Kv3.3KO gave 27.5 ± 11.0 ($n=7$) % firing, compared to 73.9 ± 19.7 % firing ($n=8$, $p = 0.0001$, Fig. 10C) for WT at 400Hz. Thus, the reduced AP firing response of LSO neurons at higher stimulus frequencies was consistent with the more severe phenotype predicted by the absent Kv3 current in Kv3.3KO.

The input–output curves plotted in Fig. 10B show high levels of variance (SD), particularly in the LSO, so although trends can be observed in the mean data, estimation of a ‘sustained firing threshold’ (defined as the stimulus current required to give 50% AP firing during the 500 ms train) was impossible, due to this high neuron-to-neuron variability, and confounded because the LSO neurons failed to sustain AP firing higher than 50% as the stimulus rate increased beyond 200 Hz, especially in the Kv3.3KO. In WT MNTB, the sustained firing threshold current significantly increased from 100 to 400 Hz stimulation: 1328 ± 433 pA ($n = 16$, $p = 0.0001$) at 100 Hz to 1475 ± 353 pA ($n = 10$) at 200 Hz compared

to 2005 ± 317 pA ($n = 9$) at 400 Hz. A similar increase in stimulus current with frequency was observed in Kv3.3KO MNTB. The full data set is presented in the Statistical Summary Table, Q22).

Following any failure to trigger an AP, the subsequent stimuli have an increased probability of evoking an AP, due to the longer interval and relative refractory period. Using data exclusively from stimulus trains with 100% AP firing to each stimulus, the latency and jitter of the evoked APs showed consistent changes. This was true at every frequency tested, but is presented here for 100 Hz stimulation. The latency of the first AP in each train for the three genotypes (WT, Kv3.1KO and Kv3.3KO) in the MNTB was: 1.06 ± 0.29 ms ($n = 8$); 0.88 ± 0.24 ms ($n = 6$); 0.89 ± 0.11 ms ($n = 10$) and for the LSO: 0.76 ± 0.11 ms ($n = 9$); 0.64 ± 0.03 ms ($n = 8$); and 0.79 ± 0.12 ms ($n = 6$), respectively. The AP latency was measured during the

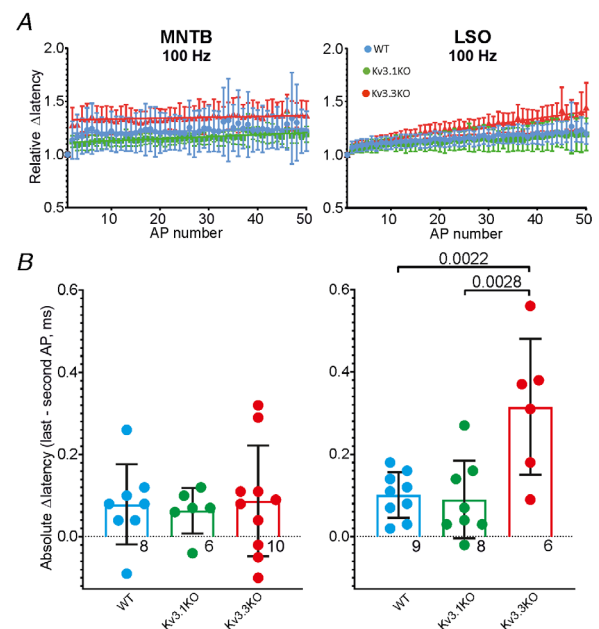


Figure 11. Channels containing Kv3.3 subunits provide enhanced latency reliability during high frequency AP firing in the LSO

AP latency fluctuations impede binocular integration and showed the greatest change in the LSO from the Kv3.3KO. A, the latency relative to the first AP of a 100 Hz train is plotted for 48 APs in a 500 ms train. In the MNTB (left) the AP latency during a 100 Hz train was relatively constant, with little cumulative change during repetitive firing and was similar between the genotypes: WT (blue), Kv3.1KO (green) and Kv3.3KO (red). In the LSO (right) the change in latency (and jitter, as indicated by the SD) increased throughout repetitive APs of the train, with the largest cumulative change in the Kv3.3KO (red). B, the cumulative latency increase is plotted as the change in latency between the second to the last AP in a 100 Hz train. The data showed no significant change in any genotype from the MNTB (left), but in the LSO (right) the latency change was significantly increased for the Kv3.3KO with respect to both the Kv3.1KO and WT; one-way ANOVA and Tukey's multiple comparison. Data from animals aged P14–P25.

100 Hz stimulus train (Fig. 11) and showed similar trends for WT and Kv3.1KO (See Summary Statistical Table, Q25 for full data). In contrast to the MNTB, the cumulative LSO latency (Fig. 11B) significantly increased from 0.101 ± 0.055 ms ($n=9$) to 0.314 ± 0.165 ms ($n=6$, $p=0.0028$) in the Kv3.3KO. Such latency changes would undermine integration of binaural inputs for sound localization.

The input–output data clearly show that loss of Kv3.3 subunits in LSO principal neurons has consequences for AP timing and in sustaining high frequency firing. This is consistent with the hypothesis that Kv3.3 subunits specifically contribute to fast spiking in the integrating binaural inputs necessary for reliable sound source localization.

Discussion

Both Kv3.1 and Kv3.3 mRNA were highly expressed in the auditory brainstem. The respective KOs constrained the subunit composition. This showed that both Kv3.1 and Kv3.3 contribute to functional Kv3 channels and compensate for the absence of the other subunit in the MNTB. In the LSO, Kv3.3 subunits were essential for functional Kv3 channels. Electrophysiological recordings support the hypothesis that Kv3 channels serve similar roles in both the MNTB and the LSO, as delayed rectifiers mediating fast AP repolarization, to support short duration APs and sustain high frequency firing. In the MNTB either Kv3.1 or Kv3.3 subunits are sufficient, but in LSO principal neurons Kv3.3 subunits must be present to sustain high-frequency firing.

Kv3 channel subunits contribute to fast action potential repolarization

Kv3 genes are widely expressed in the nervous system (Rudy *et al.* 1999; 2002) and show distinct regional expression. Kv3 channels have properties consistent with the classical ‘delayed rectifier’, in that they are activated by large depolarizations achieved during action potentials and therefore contribute to AP repolarization (Brew & Forsythe, 1995; Martina *et al.* 1998; Wang *et al.* 1998). Kv3 channels are responsible for neuronal phenotypes that exhibit high frequency firing with short duration APs (Rudy & McBain, 2001).

Identifying subunit-specific roles in native neurons is confounded by heterogeneity in channel assembly, the varied expression of subunit genes in different neuronal subtypes, accessory proteins, assembly strategies and secondary modification, such as phosphorylation (Macica & Kaczmarek, 2001; Song *et al.* 2005; Park *et al.* 2006). Recombinant expression of Kv3 subunits in cell lines provides kinetic parameters, but the recorded parameters often show considerable variability and there

is no subunit-specific pharmacology. For example, the half-activation voltages for Kv3.1 channels range between +6 and +18 mV (Grissmer *et al.* 1994; Hernandez-Pineda *et al.* 1999; Rosato-Siri *et al.* 2015; Taskin *et al.* 2015) and have steady-state half-inactivation around –32 mV (Rosato-Siri *et al.* 2015). Reported Kv3.3 half-activation varied from +8 to +30 mV, while half-inactivation ranged from +5 to –30 mV (Fernandez *et al.* 2003; Irie *et al.* 2014), with steady-state inactivation being more negative in HEK than CHO cells (Fernandez *et al.* 2003), due to selection between two N-terminal methionine start codons. This variability makes it difficult to extrapolate to the properties of native Kv3 currents in real neurons.

For example, hippocampal interneurons commonly express both Kv3.1 and Kv3.2 subunits along with Kv3.3 (Chang *et al.* 2007), while pyramidal neurons have low levels of both subunits (Martina *et al.* 1998). Martinotti cells in the somatosensory cortex express high levels of Kv3.3, Kv3.2 > Kv3.1 > Kv3.4 (Wang *et al.* 2004). In the basal ganglia, all four Kv3 subunits are expressed, but fast-spiking GABA projection neurons of the substantia nigra pars reticulata, have higher levels of Kv3.1 and Kv3.4 message, compared with slow-spiking dopamine neurons (Ding *et al.* 2011). Globus pallidus neurons (Hernandez-Pineda *et al.* 1999) and basolateral amygdala interneurons generally express both Kv3.1 and Kv3.2 (McDonald & Mascagni, 2006). Renshaw cells in the spinal cord express Kv3.1 but not Kv3.2 (Song *et al.* 2006). Purkinje neurons express Kv3.3 subunits, which have been particularly associated with the generation of complex spikes (Zagha *et al.* 2008; Veys *et al.* 2013), but they also possess Kv3.1 and Kv3.4 mRNA (with no Kv3.2 message being detected at P7, Sacco *et al.* 2006). The closest similarity to the dual expression of Kv3.1 and Kv3.3 in the auditory brainstem, is in the deep cerebellar nuclei (Hurlock *et al.* 2009) and cerebellar granule cells (Weiser *et al.* 1995; Chang *et al.* 2007; Ritzau-Jost *et al.* 2014), consistent with similarities between cerebellar and auditory brainstem circuits (Oertel & Young, 2004).

We have demonstrated a mediolateral gradient of Kv3.1 mRNA, with highest levels in the MNTB relative to the LSO. Several studies have demonstrated that Kv3.1 is tonotopically distributed across the MNTB (Wang *et al.* 1998; Li *et al.* 2001; Parameshwaran *et al.* 2001). In this qRT-PCR study we did not subdivide the nuclei, but the mediolateral gradient of Kv3.1 across the SOC as a whole is consistent with the tonotopic gradient reported within the MNTB alone. Kv3.1 also binds to the Fragile X mental retardation protein (Strumbos *et al.* 2010) which acts to suppress Kv3 protein translation. It is important to note that the activity of many ion channels, including Kv3 channels, are under activity-dependent regulation via multiple protein kinases, including casein kinase, protein kinase C and nitric oxide/PKG signalling pathways (Moreno *et al.* 2001; Song *et al.* 2005; Desai

et al. 2008; Steinert *et al.* 2008; Tong *et al.* 2010; Steinert *et al.* 2011). So such modulation is likely to influence the local Kv3 activity and need not directly change protein or mRNA levels. The ionic basis of neuronal excitability requires detailed elucidation of ion channel expression, modulation and integration with intrinsic plasticity, through activity-dependent mechanisms (Song *et al.* 2005; Tong *et al.* 2010; Gu *et al.* 2018; Hu *et al.* 2018; Petitpre *et al.* 2018).

Kv3 subunit knockout mice constrain Kv3 channel composition

Mice lacking Kv3.1 (Ho *et al.* 1997; Joho *et al.* 1999; Porcello *et al.* 2002) or Kv3.3 (Hurlock *et al.* 2008; Zagha *et al.* 2010) have very mild behavioural phenotypes while the Kv3.1/Kv3.3 double KO (Espinosa *et al.* 2001; Matsukawa *et al.* 2003) is more severe, showing ataxia, tremor, hyperactivity and reduced sleep (Espinosa *et al.* 2001; Espinosa *et al.* 2004). The Kv3.1KO displayed mild deficits in motor skills, increased acoustic startle (Ho *et al.* 1997) and enhanced gamma-frequency spectral power in the cortex (Joho *et al.* 1999). Kv3.3KO mice (Zagha *et al.* 2008) showed no change in Purkinje neuron AP half-width, but reduced numbers of 'spikelets' in their complex spike. Such mild phenotypes imply functional redundancy, as documented here in MNTB neurons and similar to that observed in reticular thalamic neurons, where Kv3.1 deletion had little impact on AP waveform (Porcello *et al.* 2002).

Deletion of Kv3.1 in MNTB neurons was reported to show much reduced outward current from a HP of -40 mV (Macica *et al.* 2003), implying that Kv3 channels lacking Kv3.1 were inactivated from holding potentials positive to rest. However, we observed no significant difference in MNTB I/V relationships from either Kv3.1KO or Kv3.3KO mice (backcrossed onto the same WT CBA/CaCrI strain) and compared with WT CBA/CaCrI controls, from HPs of -40 or -60 mV. The outward currents from both KOs were of similar magnitude to WT, implying that MNTB neurons construct Kv3 channels from both subunits and the AP durations in both KOs were consistent with functional redundancy between Kv3.1 and Kv3.3 subunits. The possibility of changes in the trafficking and sub-cellular location of channels containing Kv3.1 or Kv3.3 subunits requires further investigation, especially in regard to Kv3.3 interactions with actin and the cytoskeleton (Zhang *et al.* 2016).

The roles of Kv3.1 and Kv3.3 in the auditory brainstem

We have exploited the well-characterized auditory brainstem network responsible for sound localization in the

SOC to evaluate Kv3 subunit roles in AP waveform and firing frequency. Microsecond accuracy is required for binaural processing. This is most obvious for the interaural time difference circuit in the medial superior olive but the importance of timing is increasingly recognised for the interaural level difference pathway that involves the LSO (Ashida, *et al.* 2017; Joris & Trussell, 2018).

Both the MNTB and LSO possess mRNA for Kv3.1 and Kv3.3, supporting multiple native configurations: Kv3.1 homomers, Kv3.3 homomers or populations of Kv3.1/Kv3.3 heteromers. AP waveform was examined in the three genotypes (WT, Kv3.1KO and Kv3.3KO) which 'simplified' the native channel configuration: the Kv3.1KO had homomeric Kv3.3 channels; while the Kv3.3KO had homomeric Kv3.1 channels. Comparing MNTB neurons from each KO showed potassium currents of similar magnitude and TEA sensitivity, confirming that MNTB neurons can utilize either Kv3.1 or Kv3.3 homomeric channels for AP repolarization. The fastest AP phenotype requires channels possessing both subunits (or alternatively, channel localization was influenced by the subunit composition). In contrast, LSO AP repolarization was unchanged by deletion of Kv3.1, but was significantly slowed following deletion of Kv3.3. These data support the hypothesis that LSO neurons cannot process Kv3.1 mRNA into functional channels in the absence of Kv3.3, even though the qRT-PCR suggests that Kv3.1 mRNA is present in the LSO. We have yet to exclude the possibility that Kv3.1 subunits may contribute to LSO Kv3 channels as heteromers with Kv3.3.

The impact of the two Kv3 subunits on MNTB and LSO neuron AP firing clearly showed that the MNTB can compensate for the lack of either subunit, with no change in AP firing rate across the three genotypes. The LSO exhibited an increase in AP failures with increased firing frequency, which was exacerbated in the Kv3.3KO, and is consistent with the reduced Kv3 currents. A cumulative increase in AP latency through the train was observed in the Kv3.3KO and would compromise synaptic timing in the interaural level difference network, where latency/precision (Ford *et al.* 2015) and associated convergence of EPSPs and IPSPs are necessary for sound source localization (Pilati *et al.* 2016; Beiderbeck *et al.* 2018; Brill *et al.* 2019).

Involvement of other Kv3 subunits?

Having established the extent of expression for the four Kv3 subunits in the auditory brainstem, there are several further questions. First, immunohistochemistry hints that presynaptic and postsynaptic localization of Kv3 channel subunits may differ, and the extent to which spliced variants of Kv3.1 and Kv3.3 subunits influence the localization and function of Kv3 channels requires further

investigation. Several reports have suggested that Kv3.3 or Kv3.4 subunits could be differentially incorporated into somatic *versus* presynaptic channels in the cerebellum and spinal cord (Brooke *et al.* 2004; 2010; Rowan & Christie, 2017). But the extent to which all Kv3 subunits contribute to presynaptic AP repolarization and thus influence transmitter release is an open question. Our qRT-PCR data suggest that Kv3.4 mRNA is present in the LSO at a low level (see Fig. 2), but the presence of mRNA does not guarantee functional channel protein (as seen for Kv3.1 mRNA in the LSO of the Kv3.3KO mouse).

Both MNTB and LSO principal neurons possess voltage-gated calcium channels (Bollmann *et al.* 1998; Adam *et al.* 2001; Barnes-Davies *et al.* 2001; Jurkovicova-Tarabova *et al.* 2012; Tozer *et al.* 2012) and longer duration APs should increase Ca^{2+} influx, which in turn would influence calcium-gated potassium channels. Using barium as the charge carrier (which blocks potassium currents and does not activate calcium-gated potassium channels): LSO Ba^{2+} currents were larger than those from WT MNTB, but unchanged between the genotypes, consistent with both the KO strains having similar levels of voltage-gated calcium current to WT mice. This supports the conclusion that the activity-dependent increase in $[\text{Ca}^{2+}]_i$ is due to increased AP duration, rather than increased calcium channel density.

Development, ageing and disease

Gene expression profiles in the murine SOC show the greatest change prior to hearing onset at P12 (Ehmann *et al.* 2013). Electrophysiological studies are often conducted after P12, and synaptic function has generally matured by around P16–P21 (Steinert *et al.* 2010; Walcher *et al.* 2011; Pilati *et al.* 2016). Here the Kv3 subunit mRNA levels changed little between P9 and P35 days in this CBA/CaCrl background mouse strain, but lower and increasing expression of Kv3.1 mRNA was observed on maturation at earlier ages from P3 to P8 (Liu & Kaczmarek, 1998). A decline in neuropil Kv3.1b in 15-month-old mice have been observed in optical density measurements of antibody staining (Zettel *et al.* 2007), but other studies report Kv3 mRNA as stable (Boda *et al.* 2012).

The results of this study are pertinent to the disease mechanism of spinocerebellar ataxia type 13 (SCA13), which is caused by point mutations in Kv3.3 (see Irie *et al.* 2014; Zhang & Kaczmarek, 2016). A study of human SCA13 patients carrying an R420H mutation in Kv3.3 showed an age-dependent ataxia with deficits in sound localization (Middlebrooks *et al.* 2013). Recent studies also show that Kv3.3 inactivation is regulated by coupling of the N-terminal inactivation peptide to the actin cytoskeleton and that this may contribute to excitability changes and veil stabilization in growth cones during development (Zhang *et al.* 2016).

Auditory brainstem Kv3 channels are composed of Kv3.1 and Kv3.3 subunits, but Kv3.3 is of particular importance for functional Kv3 channels in the LSO. Future studies will determine whether localization of Kv3.3 to particular neuronal compartments (axons or presynaptic terminals) is of physiological importance. Longer APs and the resultant increased calcium influx would dramatically potentiate transmitter release and exacerbate timing errors at the synaptic level. The compromised sound localization in human SCA13 patients, likely reflects loss of Kv3 channel function in the LSO and a mouse model of this human disease mutation (Middlebrooks *et al.* 2013) would give further insights into Kv3 auditory processing and perhaps into mechanisms of neurodegeneration associated with this form of ataxia.

REFERENCES

- Adam TJ, Finlayson PG & Schwarz DW (2001). Membrane properties of principal neurons of the lateral superior olive. *J Neurophysiol* **86**, 922–934.
- Ashida G, Tollin DJ & Kretzberg J (2017). Physiological models of the lateral superior olive. ed. Theunissen FE. *PLoS Comput Biol* **13**, e1005903.
- Barnes-Davies M, Barker MC, Osmani F & Forsythe ID (2004). Kv1 currents mediate a gradient of principal neuron excitability across the tonotopic axis in the rat lateral superior olive. *Eur J Neurosci* **19**, 325–333.
- Barnes-Davies M, Owens S & Forsythe ID (2001). Calcium channels triggering transmitter release in the rat medial superior olive. *Hear Res* **162**, 134–145.
- Boda E, Hoxha E, Pini A, Montarolo F & Tempia F (2012). Brain Expression of Kv3 Subunits During Development, Adulthood and Aging and in a Murine Model of Alzheimer's Disease. *J Mol Neuroscience* **46**, 606–615.
- Bollmann JH, Helmchen F, Borst J & Sakmann B (1998). Postsynaptic Ca^{2+} influx mediated by three different pathways during synaptic transmission at a calyx-type synapse. *J Neurosci* **18**, 10409–10419.
- Brew HM & Forsythe ID (1995). Two voltage-dependent K^+ conductances with complementary functions in postsynaptic integration at a central auditory synapse. *J Neurosci* **15**, 8011–8022.
- Beiderbeck B, Myoga MH, Müller NIC, Callan AR, Friauf E, Grothe B & Pecka M (2018). Precisely timed inhibition facilitates action potential firing for spatial coding in the auditory brainstem. *Nat Commun* **9**, 1771.
- Brill SE, Janz K, Singh A & Friauf E (2019). Considerable differences between auditory medulla, auditory midbrain, and hippocampal synapses during sustained high-frequency stimulation: Exceptional vesicle replenishment restricted to sound localization circuit. *Hear Res* **381**, 107771.
- Brooke RE, Corns L, Edwards IJ & Deuchars J (2010). Kv3.3 immunoreactivity in the vestibular nuclear complex of the rat with focus on the medial vestibular nucleus: targeting of Kv3.3 neurones by terminals positive for vesicular glutamate transporter 1. *Brain Res* **1345**, 45–58.

- Brooke RE, Moores TS, Morris NP, Parson SH & Deuchars J (2004). Kv3 voltage-gated potassium channels regulate neurotransmitter release from mouse motor nerve terminals. *Eur J Neurosci* **20**, 3313–3321.
- Chang SY, Zagha E, Kwon ES, Ozaita A, Bobik M, Martone ME, Ellisman MH, Heintz N & Rudy B (2007). Distribution of Kv3.3 potassium channel subunits in distinct neuronal populations of mouse brain. *J Comp Neurol* **502**, 953–972.
- Chow A, Erisir A, Farb C, Nadal MS, Ozaita A, Lau D, Welker E & Rudy B (1999). K⁺ channel expression distinguishes subpopulations of parvalbumin- and somatostatin-containing neocortical interneurons. *J Neurosci* **19**, 9332–9345.
- Coetzee WA, Amarillo Y, Chiu J, Chow A, Lau D, McCormack T, Moreno H, Nadal MS, Ozaita A, Pountney D, Saganich M, Vega-Saenz de Miera E & Rudy B (1999). Molecular diversity of K⁺ channels. *Ann N Y Acad Sci* **868**, 233–285.
- Desai RR, Kronengold JJ, Mei JJ, Forman SAS & Kaczmarek LKL (2008). Protein Kinase C modulates inactivation of Kv3.3 channels. *J Biol Chem* **283**, 22283–22294.
- Ding S, Matta SG & Zhou F-M (2011). Kv3-like potassium channels are required for sustained high-frequency firing in basal ganglia output neurons. *J Neurophysiol* **105**, 554–570.
- Dodson PD, Barker MC & Forsythe ID (2002). Two heteromeric Kv1 potassium channels differentially regulate action potential firing. *J Neurosci* **22**, 6953–6961.
- Edelstein AD, Tsuchida MA, Amodaj N, Pinkard H, Vale RD & Stuurman N (2014). Advanced methods of microscope control using μ Manager software. *J Biol Methods* **1**, 10.
- Ehmann H, Hartwich H, Salz C, Hartmann N, Clément-Ziza M, Ushakov K, Avraham KB, Bininda-Emonds ORP, Hartmann AK, Lang P, Friauf E & Nothwang HG (2013). Time-dependent gene expression analysis of the developing superior olivary complex. *J Biol Chem* **288**, 25865–25879.
- Espinosa F, Marks G, Heintz N & Joho RH (2004). Increased motor drive and sleep loss in mice lacking Kv3-type potassium channels. *Genes Brain Behav* **3**, 90–100.
- Espinosa F, McMahon A, Chan E, Wang S, Ho CS, Heintz N & Joho RH (2001). Alcohol hypersensitivity, increased locomotion, and spontaneous myoclonus in mice lacking the potassium channels Kv3.1 and Kv3.3. *J Neurosci* **21**, 6657–6665.
- Fernandez FR, Morales E, Rashid AJ, Dunn RJ & Turner RW (2003). Inactivation of Kv3.3 potassium channels in heterologous expression systems. *J Biol Chem* **278**, 40890–40898.
- Ford MC, Alexandrova O, Cossell L, Stange-Marten A, Sinclair J, Kopp-Scheinflug C, Pecka M, Attwell D & Grothe B (2015). Tuning of Ranvier node and internode properties in myelinated axons to adjust action potential timing. *Nat Commun* **6**, 8073.
- Franken TP, Joris PX & Smith PH (2018). Principal cells of the brainstem's interaural sound level detector are temporal differentiators rather than integrators. *Elife* **7**: e33854.
- Grissmer S, Nguyen AN, Aiyar J, Hanson DC, Mather RJ, Gutman GA, Karmilowicz MJ, Auperin DD & Chandy KG (1994). Pharmacological Characterization of 5 Cloned Voltage-Gated K⁺ Channels, Types Kv1.1, Kv1.2, Kv1.3, Kv1.5, and Kv3.1, Stably Expressed in Mammalian-Cell Lines. *Mol Pharmacol* **45**, 1227–1234.
- Grothe B (2000). The evolution of temporal processing in the medial superior olive, an auditory brainstem structure. *Prog Neurobiol* **61**, 581–610.
- Gu Y, Servello D, Han Z, Lalchandani RR, Ding JB, Huang K & Gu C (2018). Balanced Activity between Kv3 and Nav Channels Determines Fast-Spiking in Mammalian Central Neurons. *iScience* **9**, 120–137.
- Hernandez-Pineda R, Chow A, Amarillo Y, Moreno H, Saganich M, Vega-Saenz de Miera EC, Hernandez-Cruz A & Rudy B (1999). Kv3.1-Kv3.2 channels underlie a high-voltage-activating component of the delayed rectifier K⁺ current in projecting neurons from the globus pallidus. *J Neurophysiol* **82**, 1512–1528.
- Ho CS, Grange RW & Joho RH (1997). Pleiotropic effects of a disrupted K⁺ channel gene: Reduced body weight, impaired motor skill and muscle contraction, but no seizures. *Proc Natl Acad Sci* **94**, 1533–1538.
- Hu H, Roth FC, Vandael D & Jonas P (2018). Complementary tuning of Na⁺ and K⁺ channel gating underlies fast and energy-efficient action potentials in GABAergic interneuron axons. *Neuron* **98**, 156–165.e156.
- Hurlock EC, Bose M, Pierce G & Joho RH (2009). Rescue of motor coordination by Purkinje cell-targeted restoration of Kv3.3 channels in Kcnc3-null mice requires Kcnc1. *J Neurosci* **29**, 15735–15744.
- Hurlock EC, McMahon A & Joho RH (2008). Purkinje-cell-restricted restoration of Kv3.3 function restores complex spikes and rescues motor coordination in Kcnc3 mutants. *J Neurosci* **28**, 4640–4648.
- Irie T, Matsuzaki Y, Sekino Y & Hirai H (2014). Kv3.3 channels harbouring a mutation of spinocerebellar ataxia type 13 alter excitability and induce cell death in cultured cerebellar Purkinje cells. *J Physiol (Lond)* **592**, 229–247.
- Johnston J, Forsythe ID & Kopp-Scheinflug C (2010). Going native: voltage-gated potassium channels controlling neuronal excitability. *J Physiol (Lond)* **588**, 3187–3200.
- Johnston J, Griffin SJ, Baker C, Skrzypiec A, Chernova T & Forsythe ID (2008). Initial segment Kv2.2 channels mediate a slow delayed rectifier and maintain high frequency action potential firing in medial nucleus of the trapezoid body neurons. *J Physiol (Lond)* **586**, 3493–3509.
- Joho RH, Ho CS & Marks GA (1999). Increased gamma- and decreased delta-oscillations in a mouse deficient for a potassium channel expressed in fast-spiking interneurons. *J Neurophysiol* **82**, 1855–1864.
- Joris PX & Trussell LO (2018). The Calyx of Held: A hypothesis on the need for reliable timing in an intensity-difference encoder. *Neuron* **100**, 534–549.
- Jurkovicova-Tarabova B, Griesemer D, Pirone A, Sinnegger-Brauns MJ, Striessnig J & Friauf E (2012). Repertoire of high voltage-activated Ca²⁺ channels in the lateral superior olive: functional analysis in wild-type, Cav1.3^(-/-), and Cav1.2DHP^(-/-) mice. *J Neurophysiol* **108**, 365–379.
- Kaczmarek LK & Zhang Y (2017). Kv3 Channels: Enablers of Rapid Firing, Neurotransmitter Release, and Neuronal Endurance. *Physiol Rev* **97**, 1431–1468.

- Kopp-Scheinflug C & Forsythe ID (2018). Integration of synaptic and intrinsic conductances shapes microcircuits in the superior olivary complex. In *The Mammalian Auditory Pathways*, Springer Handbook of Auditory Research, pp. 101–126. Springer International Publishing, Cham.
- Kopp-Scheinflug C, Pigott BM & Forsythe ID (2015). Nitric oxide selectively suppresses I_H currents mediated by HCN1-containing channels. *J Physiol (Lond)* **593**, 1685–1700.
- Li W, Kaczmarek LK & Perney TM (2001). Localization of two high-threshold potassium channel subunits in the rat central auditory system. *J Comp Neurol* **437**, 196–218.
- Lien CC & Jonas P (2003). Kv3 potassium conductance is necessary and kinetically optimized for high-frequency action potential generation in hippocampal interneurons. *J Neurosci* **23**, 2058–2068.
- Liu S & Kaczmarek LK (1998). The expression of two splice variants of the Kv3.1 potassium channel gene is regulated by different signaling pathways. *J Neurosci* **18**, 2881–2890.
- Lucas SJ, Michel CB, Marra V, Smalley JL, Hennig MH, Graham BP & Forsythe ID (2018). Glucose and lactate as metabolic constraints on presynaptic transmission at an excitatory synapse. *J Physiol*, **596**, 1699–1721.
- Macica CM & Kaczmarek LK (2001). Casein kinase 2 determines the voltage dependence of the Kv3.1 channel in auditory neurons and transfected cells. *J Neurosci* **21**, 1160–1168.
- Macica CM, HehnvonCAA, Wang L-Y, Ho C-S, Yokoyama S, Joho RH & Kaczmarek LK (2003). Modulation of the kv3.1b potassium channel isoform adjusts the fidelity of the firing pattern of auditory neurons. *J Neurosci* **23**, 1133–1141.
- Martina M, Schultz JH, Ehmke H, Monyer H & Jonas P (1998). Functional and molecular differences between voltage-gated K⁺ channels of fast-spiking interneurons and pyramidal neurons of rat hippocampus. *J Neurosci* **18**, 8111–8125.
- Matsukawa H, Wolf AM, Matsushita S, Joho RH & Knöpfel T (2003). Motor dysfunction and altered synaptic transmission at the parallel fiber-Purkinje cell synapse in mice lacking potassium channels Kv3.1 and Kv3.3. *J Neurosci* **23**, 7677–7684.
- McDonald AJ & Mascagni F (2006). Differential expression of Kv3.1b and Kv3.2 K⁺ channel subunits in interneurons of the basolateral amygdala. *Neuroscience* **138**, 537–547.
- Middlebrooks JC, Nick HS, Subramony SH, Advincula J, Rosales RL, Lee LV, Ashizawa T & Waters MF (2013). Mutation in the Kv3.3 voltage-gated potassium channel causing spinocerebellar ataxia 13 disrupts sound-localization mechanisms. *PLoS One* **8**, e76749.
- Moreno H, Vega-Saenz de Miera E, Nadal MS, Amarillo Y & Rudy B (2001). Modulation of Kv3 potassium channels expressed in CHO cells by a nitric oxide-activated phosphatase. *J Physiol (Lond)* **530**, 345–358.
- Oertel D & Young ED (2004). What's a cerebellar circuit doing in the auditory system? *Trends Neurosci* **27**, 104–110.
- Parameshwaran S, Carr CE & Perney TM (2001). Expression of the Kv3.1 potassium channel in the avian auditory brainstem. *J Neurosci* **21**, 485–494.
- Park K-S, Mohapatra DP, Misonou H & Trimmer JS (2006). Graded regulation of the Kv2.1 potassium channel by variable phosphorylation. *Science* **313**, 976–979.
- Perney TM, Marshall J, Martin KA, Hockfield S & Kaczmarek LK (1992). Expression of the mRNAs for the Kv3.1 potassium channel gene in the adult and developing rat brain. *J Neurophysiol* **68**, 756–766.
- Petitpre C, Wu H, Sharma A, Tokarska A, Fontanet P, Wang Y, Helmbacher F, Yackle K, Silberberg G, Hadjaj S & Lallemand F (2018). Neuronal heterogeneity and stereotyped connectivity in the auditory afferent system. *Nat Commun* **9**, 3691.
- Pfaffl MW (2001). A new mathematical model for relative quantification in real-time RT-PCR. *Nucleic Acids Res.* **29**(9): e45.
- Pilati N, Linley DM, Selvaskandan H, Uchitel O, Hennig MH, Kopp-Scheinflug C & Forsythe ID (2016). Acoustic trauma slows AMPA receptor-mediated EPSCs in the auditory brainstem, reducing GluA4 subunit expression as a mechanism to rescue binaural function. *J Physiol (Lond)* **594**, 3683–3703.
- Porcello DM, Ho C-S, Joho RH & Huguenard JR (2002). Resilient RTN fast spiking in Kv3.1 null mice suggests redundancy in the action potential repolarization mechanism. *J Neurophysiol* **87**, 1303–1310.
- Ritzau-Jost A, Delvendahl I, Rings A, Byczkowitz N, Harada H, Shigemoto R, Hirrlinger J, Eilers J & Hallermann S (2014). Ultrafast action potentials mediate kilohertz signaling at a central synapse. *Neuron* **84**, 152–163.
- Rosato-Siri MD, Zambello E, Mutinelli C, Garbati N, Benedetti R, Aldegheri L, Graziani F, Virginio C, Alvaro G & Large CH (2015). A Novel Modulator of Kv3 Potassium Channels Regulates the Firing of Parvalbumin-Positive Cortical Interneurons. *J Pharmacol Exp Ther* **354**, 251–260.
- Rowan MJM & Christie JM (2017). Rapid State-Dependent Alteration in Kv3 Channel Availability Drives Flexible Synaptic Signaling Dependent on Somatic Subthreshold Depolarization. *Cell Rep* **18**, 2018–2029.
- Rudy B & McBain CJ (2001). Kv3 channels: voltage-gated K⁺ channels designed for high-frequency repetitive firing. *Trends Neurosci* **24**, 517–526.
- Rudy B, Chow A, Lau D, Amarillo Y, Ozaita A, Saganich M, Moreno H, Nadal MS, Hernandez-Pineda R, Hernandez-Cruz A, Erisir A, Leonard C & Vega-Saenz de Miera E (1999). Contributions of Kv3 channels to neuronal excitability. *Ann N Y Acad Sci* **868**, 304–343.
- Rudy B, Chow A, Lau D, Amarillo Y, Ozaita A, Saganich M, Moreno H, Nadal MS, Pineda RH, Cruz AH, Erisir A, Leonard C & Vega-Saenz de Miera E (2002). Contributions of Kv3 channels to neuronal excitability. *Ann N Y Acad Sci* **868**, 304–343.
- Schnupp JWH & Carr CE (2009). On hearing with more than one ear: lessons from evolution. *Nat Neurosci* **12**, 692–697.
- Sacco T, De Luca A & Tempia F (2006). Properties and expression of Kv3 channels in cerebellar Purkinje cells. *Mol Cell Neurosci* **33**, 170–179.
- Song P, Yang Y, Barnes-Davies M, Bhattacharjee A, Hamann M, Forsythe ID, Oliver DL & Kaczmarek LK (2005). Acoustic environment determines phosphorylation state of the Kv3.1 potassium channel in auditory neurons. *Nat Neurosci* **8**, 1335–1342.

- Song Z-M, Hu J, Rudy B & Redman SJ (2006). Developmental changes in the expression of calbindin and potassium-channel subunits Kv3.1b and Kv3.2 in mouse Renshaw cells. *Neuroscience* **139**, 531–538.
- Steinert JR, Kopp-Scheinflug C, Baker C, Challiss RAJ, Mistry R, Hausteiner MD, Griffin SJ, Tong H, Graham BP & Forsythe ID (2008). Nitric oxide is a volume transmitter regulating postsynaptic excitability at a glutamatergic synapse. *Neuron* **60**, 642–656.
- Steinert JR, Postlethwaite M, Jordan MD, Chernova T, Robinson SW & Forsythe ID (2010). NMDAR-mediated EPSCs are maintained and accelerate in time course during maturation of mouse and rat auditory brainstem in vitro. *J Physiol (Lond)* **588**, 447–463.
- Steinert JR, Robinson SW, Tong H, Hausteiner MD, Kopp-Scheinflug C & Forsythe ID (2011). Nitric oxide is an activity-dependent regulator of target neuron intrinsic excitability. *Neuron* **71**, 291–305.
- Sterenborg JC, Pilati N, Sheridan CJ, Uchitel OD, Forsythe ID & Barnes-Davies M (2010). Lateral olivocochlear (LOC) neurons of the mouse LSO receive excitatory and inhibitory synaptic inputs with slower kinetics than principal neurons. *Hear Res* **270**, 119–126.
- Strumbos JG, Brown MR, Kronengold J, Polley DB & Kaczmarek LK (2010). Fragile X mental retardation protein is required for rapid experience-dependent regulation of the potassium channel Kv3.1b. *J Neurosci* **30**, 10263–10271.
- Taskin B, SchoubyevonNL, Sheykhzade M, Bastlund JF, Grunnet M & Jespersen T (2015). Biophysical characterization of KV3.1 potassium channel activating compounds. *Eur J Pharmacol* **758**, 164–170.
- Tollin DJ (2003). The lateral superior olive: a functional role in sound source localization. *Neuroscientist* **9**, 127–143.
- Tong H, Steinert JR, Robinson SW, Chernova T, Read DJ, Oliver DL & Forsythe ID (2010). Regulation of Kv channel expression and neuronal excitability in rat medial nucleus of the trapezoid body maintained in organotypic culture. *J Physiol (Lond)* **588**, 1451–1468.
- Tozer AJB, Forsythe ID & Steinert JR (2012). Nitric oxide signalling augments neuronal voltage-gated L-type (Cav1 and P/Q-type Cav2.1) channels in the mouse medial nucleus of the trapezoid body. *PLoS One* **7**, e32256.
- Trimmer JS (2015). Subcellular localization of K⁺ channels in mammalian brain neurons: remarkable precision in the midst of extraordinary complexity. *Neuron* **85**, 238–256.
- Veys K, Snyder D & De Schutter E (2013). Kv3.3b expression defines the shape of the complex spike in the Purkinje cell. *Front Cell Neurosci* **7**, 205.
- Walcher J, Hassfurth B, Grothe B & Koch U (2011). Comparative post-hearing development of inhibitory inputs to the lateral superior olive in gerbils and mice. *J Neurophysiol* **106**, 1443–1453.
- Wang LY, Gan L, Forsythe ID & Kaczmarek LK (1998). Contribution of the Kv3.1 potassium channel to high-frequency firing in mouse auditory neurons. *J Physiol (Lond)* **509**, 183–194.
- Wang Y, Toledo-Rodriguez M, Gupta A, Wu C, Silberberg G, Luo J & Markram H (2004). Anatomical, physiological and molecular properties of Martinotti cells in the somatosensory cortex of the juvenile rat. *J Physiol (Lond)* **561**, 65–90.
- Weiser M, Bueno E, Sekirnjak C, Martone ME, Baker H, Hillman D, Chen S, Thornhill W, Ellisman M & Rudy B (1995). The potassium channel subunit Kv3.1b is localized to somatic and axonal membranes of specific populations of CNS neurons. *J Neurosci* **15**, 4298–4314.
- Weiser M, Vega-Saenz de Miera E, Kentros C, Moreno H, Franzen L, Hillman D, Baker H & Rudy B (1994). Differential expression of Shaw-related K⁺ channels in the rat central nervous system. *J Neurosci* **14**, 949–972.
- Zagha E, Lang EJ & Rudy B (2008). Kv3.3 channels at the Purkinje cell soma are necessary for generation of the classical complex spike waveform. *J Neurosci* **28**, 1291–1300.
- Zagha E, Manita S, Ross WN & Rudy B (2010). Dendritic Kv3.3 Potassium Channels in Cerebellar Purkinje Cells Regulate Generation and Spatial Dynamics of Dendritic Ca²⁺ Spikes. *J Neurophysiol* **103**, 3516–3525.
- Zettel ML, Zhu X, O'Neill WE & Frisina RD (2007). Age-related decline in Kv3.1b expression in the mouse auditory brainstem correlates with functional deficits in the medial olivocochlear efferent system. *J Assoc Res Otolaryngol* **8**, 280–293.
- Zhang Y & Kaczmarek LK (2016). Kv3.3 potassium channels and spinocerebellar ataxia. *J Physiol (Lond)* **594**, 4677–4684.
- Zhang Y, Zhang X-F, Fleming MR, Amiri A, El-Hassar L, Surguchev AA, Hyland C, Jenkins DP, Desai R, Brown MR, Gazula V-R, Waters MF, Large CH, Horvath TL, Navaratnam D, Vaccarino FM, Forscher P & Kaczmarek LK (2016). Kv3.3 Channels Bind Hax-1 and Arp2/3 to Assemble a Stable Local Actin Network that Regulates Channel Gating. *Cell* **165**, 434–448.
- Zheng QY, Johnson KR & Erway LC (1999). Assessment of hearing in 80 inbred strains of mice by ABR threshold analyses. *Hear Res* **130**, 94–107.

Additional information

Competing interests

The authors declare no competing interests. All authors have approved the final version of the manuscript and agree to be accountable for the work. Only authors who qualify for authorship have been listed.

Funding

This work was funded by a project grant from the BBSRC (NC, MA, JRS, IDF), a BBSRC PhD Case Studentship (AR/IDF); MRC intramural funding (SWR), and a PhD Scholarship (DL/IDF) from Action on Hearing Loss (AoHL). SMW received an Erasmus+ traineeship from Freie University, Berlin Germany.

Acknowledgements

Thanks to personnel of the Preclinical Research Facility (PRF) for conducting mouse genetics, breeding and animal maintenance; and to the University of Leicester Genomics Facility for contributions to the quantitative RT-PCR.

Author contributions

The electrophysiology experiments were conducted by NC, DL and AR with additional data from JRS and CKS; immunohistochemistry, laser microdissection, qRT-PCR and western blots were conducted by SWR and MA with additional input from AR, and the Leicester Genomics facility. Calcium imaging was conducted by NC with assistance from AR, VM and JRS. Data and analysis of action potential trains was conducted by VC, SMW, NC and JRS. All authors contributed to analysis and interpretation, with JRS leading on integrating the data set for statistical analysis and figure construction. IDF supervised the project and wrote the manuscript with input from all authors.

Keywords

auditory system, potassium channel, voltage clamp

Supporting information

Additional supporting information may be found online in the Supporting Information section at the end of the article.

Statistical Summary Document